NASA Contractor Report 202331

SiC Recession Due to SiO_2 Scale Volatility Under Combustor Conditions

Raymond Craig Robinson
NYMA, Inc.
Brook Park, Ohio

March 1997

Prepared for
Lewis Research Center
Under Contract NAS3–27186

National Aeronautics and
Space Administration

Trade names or manufacturers' names are used in this report for identification only. This usage does not constitute an official endorsement, either expressed or implied, by the National Aeronautics and Space Administration.

SiC RECESSION DUE TO SiO_2 SCALE VOLATILITY UNDER COMBUSTOR CONDITIONS

by

RAYMOND CRAIG ROBINSON

Submitted in partial fulfillment of the requirements

for the Degree of Master of Science

Thesis Advisor: Dr. John J. Lewandowski

Department of Materials Science and Engineering

CASE WESTERN RESERVE UNIVERSITY

May 1996

SiC RECESSION DUE TO SiO_2 SCALE VOLATILITY UNDER COMBUSTOR CONDITIONS

Abstract

by

RAYMOND C. ROBINSON

One of today's most important and challenging technological problems is the development of advanced materials and processes required to design and build a fleet of supersonic High Speed Civil Transport (HSCT) airliners, a follow-up to the Concorde SST. The innovative combustor designs required for HSCT engines will need high-temperature materials with long-term environmental stability. Higher combustor liner temperatures than today's engines and the need for lightweight materials will require the use of advanced ceramic-matrix composites (CMC's) in hot-section components. The HSCT is just one example being used to demonstrate the need for such materials. This thesis evaluates silicon carbide (SiC) as a potential base material for HSCT and other similar applications.

Key issues are the environmental durability for the materials of interest. One of the leading combustor design schemes leads to an environment which will contain both oxidizing and reducing gas mixtures. The concern

is that these environments may affect the stability of the silica (SiO_2) scale on which SiC depends for environmental protection. A unique High Pressure Burner Rig (HPBR) was developed to simulate the combustor conditions of future gas turbine engines, and a series of tests were conducted on commercially available SiC material. These tests are intended as a feasibility study for the use of these materials in applications such as the HSCT.

Linear weight loss and surface recession of the SiC is observed as a result of SiO_2 volatility for both fuel-lean and fuel-rich gas mixtures. These observations are compared and agree well with thermogravimetric analysis (TGA) experiments. A strong Arrhenius-type temperature dependence exists. In addition, the secondary dependencies of pressure and gas velocity are defined. As a result, a model is developed to enable extrapolation to points outside the experimental space of the burner rig, and in particular, to potential gas turbine engine conditions.

Acknowledgements

The most important acknowledgements go to Mr. Leonard Bunyak and Mr. James Nickel for their mechanical support and operation of the experimental equipment. Without their everyday cooperation this work would never have been completed. I would also like to recognize Dr. James Smialek for his technical guidance and objective review. Jim is a recognized leader at the NASA Lewis Research Center in the area of oxidation and was instrumental in developing the idea of normalized recession.

Other contributors were Mr. Dennis Fox, Dr. Nathan Jacobson, and Dr. Elizabeth Opila whom are all part of the Environmental Durability Branch at NASA LeRC. Nate was essential in providing degradation mechanisms, chemical reactions, and thermodynamic considerations. Dennis and Beth contributed in the areas of oxidation kinetics and thermogravimetric analyses for both model rich and model lean gas mixtures. Lastly, Mr. Chuck Barrett is recognized for his help with the multi-linear regression analysis.

A special thanks to Mr. Carl Stearns who served as a mentor to me during the development of the experimental facility and early part of materials testing. Carl not only hired me for this work during his reign as branch chief, but worked as my NYMA, Inc. associate after his retirement from civil service. His tutorship in the area of burner rig combustion and general rig design was invaluable in building a world-class test facility.

Table of Contents

List of Figures

List of Tables

1.0 INTRODUCTION

The High Speed Civil Transport (HSCT) is a next generation commercial supersonic aircraft that would travel at speeds more than twice the speed of sound. It would be capable of carrying 300 passengers from Los Angeles to Tokyo in under 4.5 hours, compared to the current subsonic commercial flight time of 10.5 hours. Intended to be an improvement over its predecessor, the Concorde, this initiative is of international importance and has received much media coverage throughout the business and aerospace community [1,2]. Studies have shown that there is a large potential market for this Mach 2.4 HSCT aircraft with a 5000-6000 nautical mile range. However the aircraft must first overcome major technology barriers to become a reality. Probably the biggest concern is environmental, which is derived primarily from nitrous oxide (NOx) emission considerations [3,4].

For the HSCT to become a reality, radical changes must be incorporated into combustor design to reduce NOx emissions. The material requirements for reduced NOx combustors will be radically different from that of current combustors. In general, burning at lower temperatures away from stoichiometric fuel-to-air ratios limits NOx formation. One innovative combustor design will make use of a primary fuel-rich combustion zone to initiate lower flame temperatures. However, this prohibits the use of film cooling from bypass air and allows only backside cooling. Conventional fuel-

lean combustion zones must also be considered. Thus, the combustor liner will operate in both oxidizing and oxygen-deficient environments and at very high temperatures. Exact material temperatures are not known, but the open literature [5] has quoted maximum use temperatures as high as 1650°C. In addition, the projected lifetime of the HSCT combustor is approximately 18,000 hrs, making long-term high temperature environmental durability a critical factor in its development. Finally, candidate materials must offer low density, thus advanced ceramics have emerged as leading candidate materials.

How candidate materials endure in complex environments, such as the HSCT combustor, is of fundamental importance to the materials development. Previous work at the NASA Lewis Research Center focussed on the environmental durability of some potential materials. The base ceramic materials initially under consideration included both nonoxides (SiC, Si_3N_4, $MoSi_2$, AlN) and oxides (Al_2O_3, $3(Al_2O_3)\cdot 2(SiO_2)$, $TiO_2\cdot Al_2O_3$, $Y_2O_3\cdot 2(ZrO_2)$). Theoretical studies by Jacobson [6] identified potential degradation routes and maximum use temperatures for many of the initial candidate materials. Of these, SiC is most promising due in part to its high thermal conductivity, and has been chosen for further evaluation.

One potential problem identified is SiO_2 scale volatility and corresponding recession of SiC under rich-burn combustor operation at the temperatures of interest to future engines. Theories have been proposed and

addressed both analytically and experimentally with furnace testing, but they have not been tested under actual combustor conditions. The focus of this work is two-fold: 1) to develop experimental capabilities which closely simulate the chemical and thermal environments of future combustor designs and 2) address the concerns regarding SiO_2 volatility and SiC recession for both fuel-rich and fuel-lean gas mixtures. Rich-burn and lean-burn test matrices were completed in a High Pressure Burner Rig (HPBR) with monolithic SiC materials to define the rate of material loss. The effect of temperature, pressure, gas velocity, and sample orientation are all discussed. The goal is that accomplishment of these tasks will determine the usefulness of SiC in high temperature materials applications such as the HSCT combustor and contribute to future materials development.

2.0 BACKGROUND

2.1 Global Environmental Issues

A large fleet of HSCTs flying at high altitudes will emit significant amounts of combustion products, especially nitrous oxides (NOx), because of the high combustion temperatures required for the engine cycles. NOx emissions produced by gas turbine engines can have a severe impact on atmospheric conditions. At the high cruise altitudes (above 60,000 ft.) of the HSCT, NOx does indeed act as a catalyst for ozone destruction. While today's combustors produce approximately 30-45 grams of NOx per kilogram of fuel burned, the goal for the HSCT is less than 5 grams of NOx for the same fuel burned [3,4,5]. The challenge at hand is to reduce NOx emissions to as little as 10% of the volume emitted by conventional airliners.

At this point, it is helpful to briefly discuss both the formation of NOx and methods to control it. To begin, NOx is a product of nitrogen and oxygen combined at elevated temperature. Its formation is strongly dependent on equivalence ratio (ϕ), flame temperature, and time spent at elevated temperature [3,7]. Equivalence ratio is a normalized fuel-to-air ratio. The variation of NOx with equivalence ratio is shown in Figure 2.1. By avoiding the stoichiometric regions ($\phi = 1$) and targeting those shaded in Figure 2.1, NOx formation will be minimized. This is because the formation of NOx is greatest at the highest flame temperatures, which also coincide

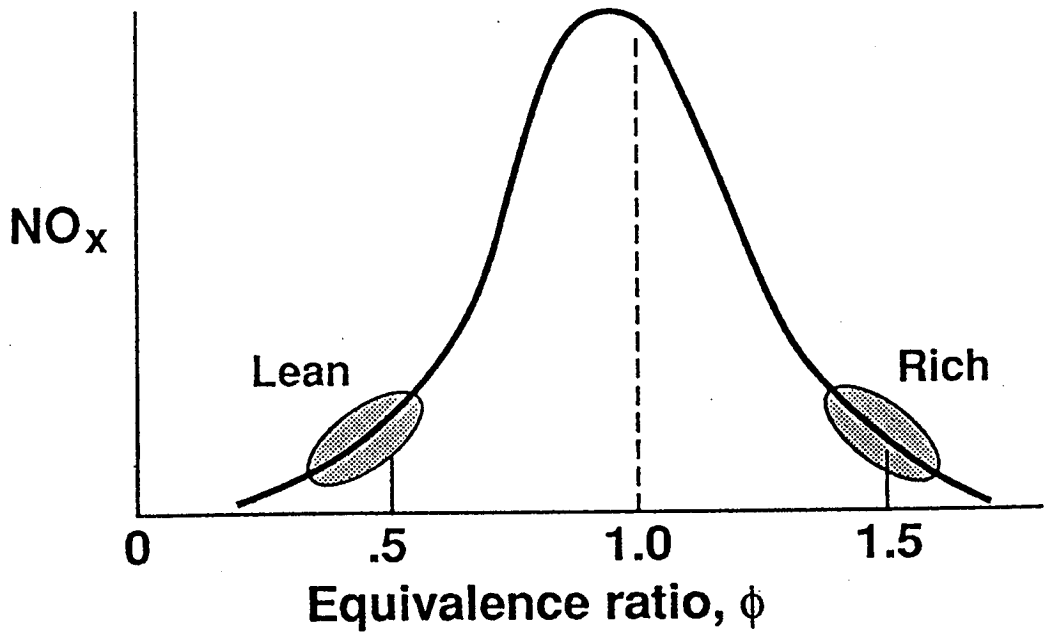

Figure 2.1 Dependency of nitrous oxides (NOx) on equivalence ratio (ϕ), where lean-burn $\phi < 1$ and rich-burn $\phi > 1$.

$\phi = 1$. In addition, NOx emissions can also be theoretically minimized by limiting the combustion process to short residence time at elevated temperature. Residence time is generally determined by the overall length of the combustor.

2.2 Combustor Environments

Given the environmental challenge, the key issue in developing an environmentally acceptable HSCT is to produce a combustor that substantially reduces NOx emissions by a factor of 8-10. To accomplish this, the RQL[1] combustor is one concept currently under consideration.

2.2.1 Advanced Combustor Concepts

The discussion will now focus on the RQL design and the combustor environments which make this concept unique. The RQL concept [5,6] addresses NOx formation by arranging a primary fuel-rich zone ($\phi > 1$) in series with a secondary fuel-lean zone ($\phi < 1$). The two combustion regions are separated by a "quick-quench" section. The arrangement and size comparison of these three regions are illustrated in Figure 2.2 [6]. Combustion is initiated in the fuel-rich zone with equivalence ratios between 1.2 and 1.8. Here, low flame temperatures and inadequate oxygen inhibit the formation of NOx. Admission of liner cooling into the fuel-rich zone is prohibited to avoid local hot spots and the formation of NOx. However,

---

[1]The Rich-burn Quick-quench Lean-burn combustor concept proposed by Pratt & Whitney Aircraft.

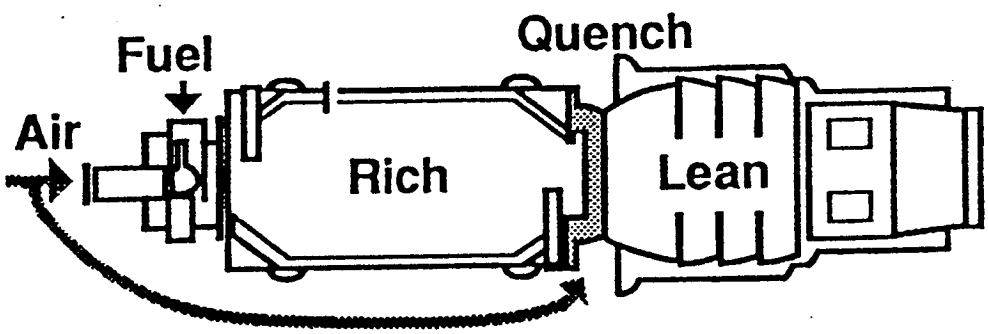

Figure 2.2 The Rich-burn Quick-quench Lean-burn (RQL) combustor concept [6].

large quantities of CO, soot, and smoke are formed. The quick-quench zone represents a step change in gas composition and temperature. Here, excess air is added very rapidly over a short distance to avoid extended residence time at high temperatures as the mixture passes through stoichiometric conditions. Combustion is completed in the lean-burn zone ($\phi \sim 0.6$), where the unwanted constituents are consumed.

2.2.2 Gas Chemistry and Thermal Environment

The combustion gas composition and adiabatic flame temperature for jet fuel at thermodynamic equilibrium is shown as a function of equivalence ratio in Figures 2.3 and 2.4, respectively [6]. The flame temperature is highest under stoichiometric conditions ($\phi = 1$). Note, the adiabatic flame temperature is a maximum temperature, and actual gas temperatures will be lower due to heat losses in the real system. Both RQL combustion regions consist of large amounts of N_2 and the combustion products CO_2 and H_2O. The amounts of O_2, CO, and H_2 vary substantially as a function of (ϕ). Fuel-lean mixtures contain a large amount of O_2 and small amounts of CO and H_2 as compared to fuel-rich mixtures, where the opposite occurs.

2.3 Materials Issues

SiC materials have always been at the forefront in the development of the advanced ceramics that will be needed to meet the HSCT requirements. Selecting a material is usually based on the best combination of environmental durability, mechanical properties, and physical properties.

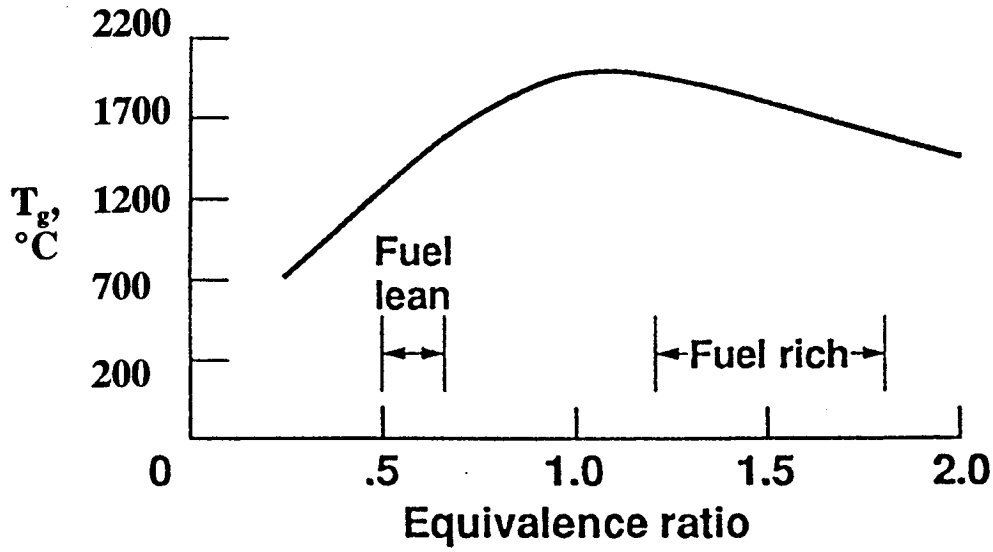

Figure 2.3 Adiabatic flame temperature vs equivalence ratio with RQL fuel-lean and fuel-rich regimes shown.

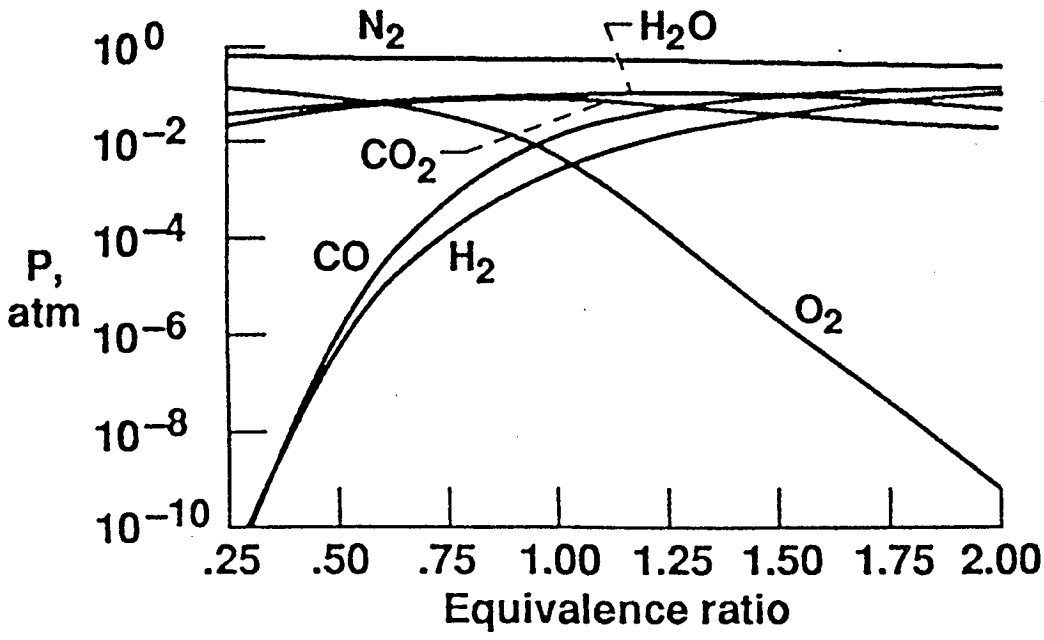

Figure 2.4 Combustor gas composition vs equivalence ratio [6].

The silicon-based materials typically seem to offer more desirable thermal conductivities and mechanical properties than the other ceramic systems. However, they generally do not have the best environmental durability when compared to other ceramics such as oxides [8].

2.3.1 SiC Degradation Mechanisms

Jacobson [6] concluded that the two major degradation routes for SiC materials are oxidation and vaporization. SiC can form SiO_2 scales in both the fuel-lean and fuel-rich environments. The question left unanswered was whether or not these scales would act as slow-growing, protective oxides. Oxidation is difficult to model because both cycling effects and water vapor are expected to play a major role. Vaporization, or reactions to form volatile products, may also occur with the growing oxide scale. Here, material loss is likely to be an issue, and maximum use temperatures were calculated [6]. In either case, it is difficult to extrapolate existing short-term furnace data to very long times and the complex environments of the HSCT.

Thus, any conclusions as to how SiC materials will behave in the environments such as the HSCT lack experimental verification. This emphasizes the need for burner rig testing, which best simulates the harsh environments of an actual combustor and is the purpose of this report. SiC materials must be exposed to actual rich-burn and lean-burn combustor environments so that previously predicted material loss rates and maximum use temperatures can be verified or more realistically defined.

2.3.2 Chemical Reactions

2.3.2.1 Fuel-Lean Mixtures

In a typical fuel-lean environment (10%O_2-8%H_2O-7%CO_2-bal.%N_2 @ $\phi = 0.5$), SiC is initially expected to exhibit good durability due to the formation of a protective silica scale with a low parabolic growth rate [9]. Figure 2.5 gives the parabolic rate constants for silica in pure oxygen compared to other oxides. Here, silica exhibits a slow growth rate and low activation energy. For temperatures above 1000°C, the silica scale is actually slower growing than alumina, which is the most common protective oxide on superalloys.

SiO_2 will form as thin, protective scales in dry oxygen and under isothermal conditions according to:

$$SiC + 1.5O_2(g) = SiO_2 + CO(g) \qquad (2.1)$$

However, O_2 is not the only oxidant present. Two other reactions are possible with SiC in these fuel-lean combustion gases. They occur as:

$$SiC + 3H_2O(g) = SiO_2 + 3H_2(g) + CO(g) \qquad (2.2)$$

$$SiC + 3CO_2(g) = SiO_2 + 4CO(g) \qquad (2.3)$$

The formation of this stable SiO_2 film is referred to as "passive oxidation". Experiments (unpublished) by Nguyen [10] at NASA LeRC have shown that the reaction of SiC with H_2O (Equation 2.2) is the more favorable oxidation step. Figure 2.6 gives the oxidation kinetics of CVD SiC at 1200°C for the oxidants H_2O, O_2, and CO_2. Here, the oxidation rate with H_2O is clearly

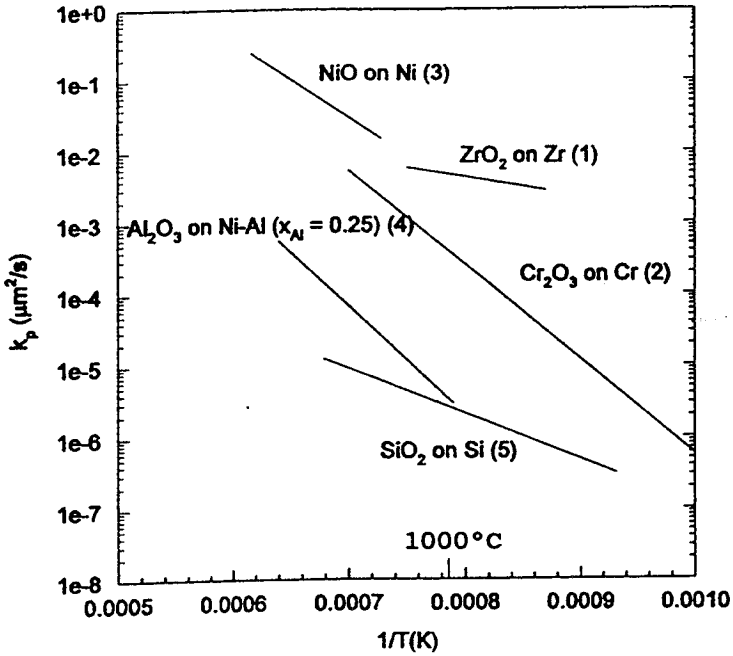

Figure 2.5 Parabolic rate constants for some common oxides [9].

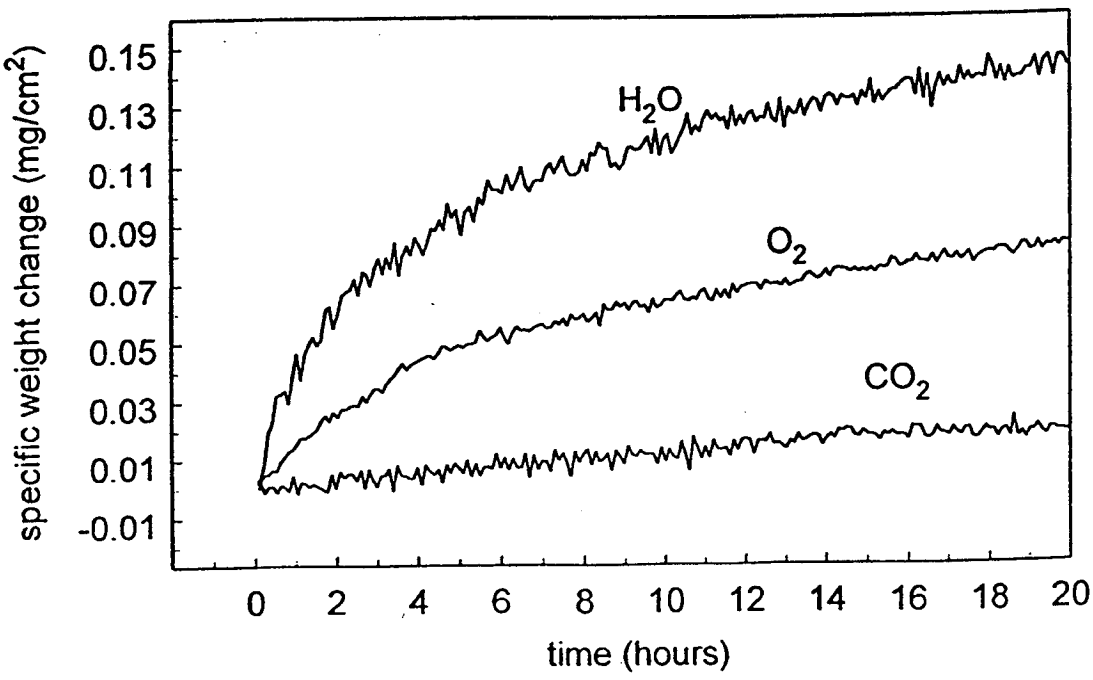

Figure 2.6 Oxidation kinetics of CVD SiC at 1200°C for the oxidants H_2O, O_2, and CO_2 [10].

faster as compared to O_2 and CO_2. Assuming a protective oxide scale has been formed via one of the above reactions, one must now consider the vaporization of that oxide. SiO_2 is known to vaporize to form SiO(g) and O_2(g), or it can reduce directly to SiO_2(g). Under fuel-lean conditions, Jacobson [6] has calculated a maximum use temperature approaching 1800°C for silica as a result of this material loss. This is based on potential RQL conditions and an acceptable material loss rate equal to 254 μm (10 mils)/10,000 hr.

Related to this is the possible volatilization of SiO_2 due to the water vapor, as nearly all oxides form some type of volatile hydroxide species. It has been known that steam enhances Si oxidation [11], with the parabolic rate constant proportional to the amount of water vapor in the gas stream. However, silica is also known to be volatile in the presence of water vapor. This is important because both rich-burn and lean-burn environments of the HSCT, in general, will contain about 10% steam. Gaseous hydrated Si species have previously been suggested for observations in which silica coupons rapidly lost weight in the presence of steam [12]. The exact Si-O-H species had been unknown until recent transpiration experiments [13] indicated a $[P(H_2O)]^2$ dependance, suggesting $Si(OH)_4$ formation:

$$SiO_2 + 2H_2O(g) = Si(OH)_4(g) \qquad (2.4)$$

Initial unpublished experiments at NASA LeRC by Lee and Jacobson on a silica coupon at 1300°C in 10% water vapor and oxygen did not

indicate evidence of volatility due to this reaction. However, testing under 1 atm test conditions may have contributed to the lack of volatility. From Hashimoto's data [13] at 1150°C, the vapor pressure of $Si(OH)_4$ is approximately $2x10^{-8}$ atm and $2x10^{-6}$ atm for 0.1 and 1.0 atm H_2O, respectively. Figure 2.7 shows the vapor pressure of $Si(OH)_4$ for 1 atm and 0.1 atm of water vapor [14].

For a 1 atm combustor with 10% water vapor, the amount of water [$P(H_2O) = 0.1$ atm] will generate an insignificant amount of $Si(OH)_4$. At higher total pressures, the total amount of steam is quite significant. In a 10 atm combustor with 10% water vapor, there is enough water vapor [$P(H_2O) = 1$ atm] to generate much more $Si(OH)_4$. This has been confirmed in more recent experiments at NASA Lewis. The $Si(OH)_3^+$ ion has been observed in a specialized sampling mass spectrometer [15], which is most likely a fragment of the $Si(OH)_4(g)$ molecule.

2.3.2.2 Fuel-Rich Mixtures

Under rich-burn conditions, oxidation is still possible, and the reaction is the same as with lean-burn conditions. As shown in Figure 2.4, a typical rich-burn environment (6%H_2-12%H_2O-12%CO-5%CO_2-bal%N_2 @ $\phi = 1.5$) contains only small amounts of O_2. However, the gases still contain significant amounts of the oxidants H_2O and CO_2. H_2O is again the major oxidant, and SiC is expected to oxidize as Equation 2.2. The volatile species of vaporization, $Si(OH)_4$, may also be the same in both fuel-rich and fuel-lean

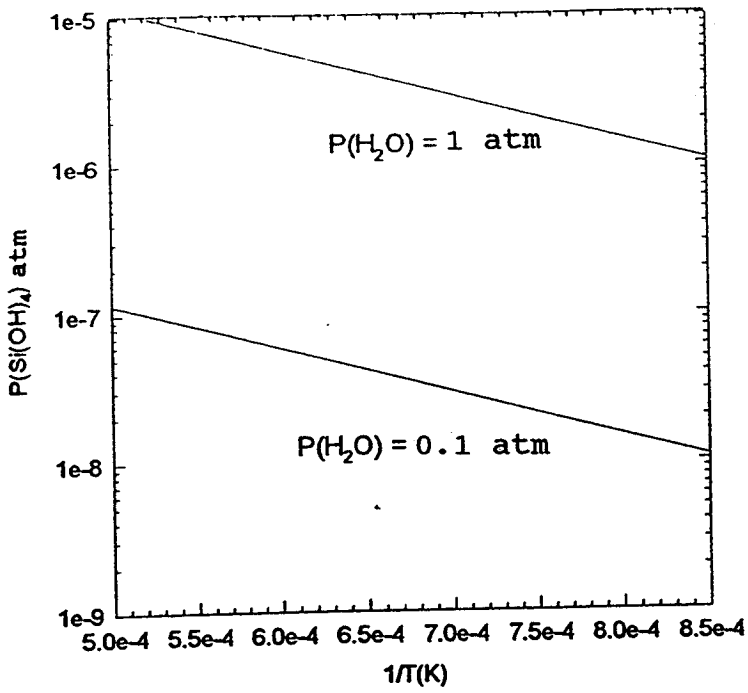

Figure 2.7 Vapor pressures of $Si(OH)_4$ above SiO_2 [14], calculated from reference [13].

environments, with additional species possible in fuel-rich. As mentioned, large amounts of the reactants H_2 and CO are also present in these fuel-rich gas mixtures. The fuel-rich combustor becomes an oxidizing/reducing mixture of H_2O/H_2 and CO_2/CO gases. Thus a potential mechanism for SiC recession occurs when a stable SiO_2 layer forms, but there are reducing gases present to simultaneously reduce the scale to SiO(g) [16].

The concerns for the stability of the silica scale are: 1) with H_2O as the primary oxidant, will it be as protective and dense as a scale grown in O_2, and 2) how will the reducing agents of H_2 and CO affect the scale? In fuel-rich mixtures, vaporization of SiO_2 could occur as simple vaporization or as a reaction with water vapor to form a volatile hydroxyl species as with fuel-lean mixtures. The formation of $Si(OH)_4$ via Equation 2.4 may also occur, or other volatiles such as $SiO(OH)_x$ may also play a role. However, another serious concern is the reduction to a lower, volatile oxide. The reduction portion, in which linear kinetics are exhibited, occurs as one of the following:

$$SiO_2 + H_2(g) = SiO(g) + H_2O(g) \qquad \textbf{(2.5)}$$

$$SiO_2 + CO(g) = SiO(g) + CO_2(g) \qquad \textbf{(2.6)}$$

Using this oxidizing/reducing mechanism, the same anticipated HSCT conditions, and acceptable material loss rate, Jacobson [6] calculated the maximum use temperature for fuel-rich environments to be approximately 1500°C. This is significantly less than the fuel-lean limit of 1800°C.

2.3.3 TGA Results on SiC

2.3.3.1 Model Lean Conditions

The oxidation kinetics of CVD SiC in the presence of water vapor have been well documented by Opila and Hann [17]. Here, the kinetics were followed by thermogravimetric analysis (TGA) in a 50%H_2O-50%O_2 gas mixture flowing at 4.4 cm/s for temperatures that ranged from 1200-1400°C. Figure 2.8 shows one such trace of the as-received SiC. Overall, initial weight gain ($k_p = 2.7x10^{-3}$ mg/cm^2-hr) is followed by linear weight loss ($k_l = 3.5x10^{-3}$ mg/cm^2-hr) which clearly indicates the formation of a volatile Si-O-H molecule, namely $Si(OH)_4$. This simultaneous oxidation behavior and linear volatilization lead to what is referred as "paralinear kinetics".

Early experiments did not result in observed weight loss, again due to low water vapor pressures. Tested under 1 atm conditions, 10% water vapor resulted in only negligible amounts of $Si(OH)_4$. However, by increasing the water vapor to 50%, the furnace more accurately modeled an actual combustor at increased total pressures. As a result, the paralinear weight change kinetics were observed as the water vapor oxidized the SiC as Equation 2.2 and simultaneously volatilized the scale as Equation 2.4.

2.3.3.2 Model Rich Conditions

The oxidation kinetics of CVD SiC have also been measured for model rich TGA conditions. Fox et.al. [18] measured the kinetics in a 4%H_2-13%H_2O-10%CO-7%CO_2-balance N_2 gas mixture flowing at 0.44 cm/s for

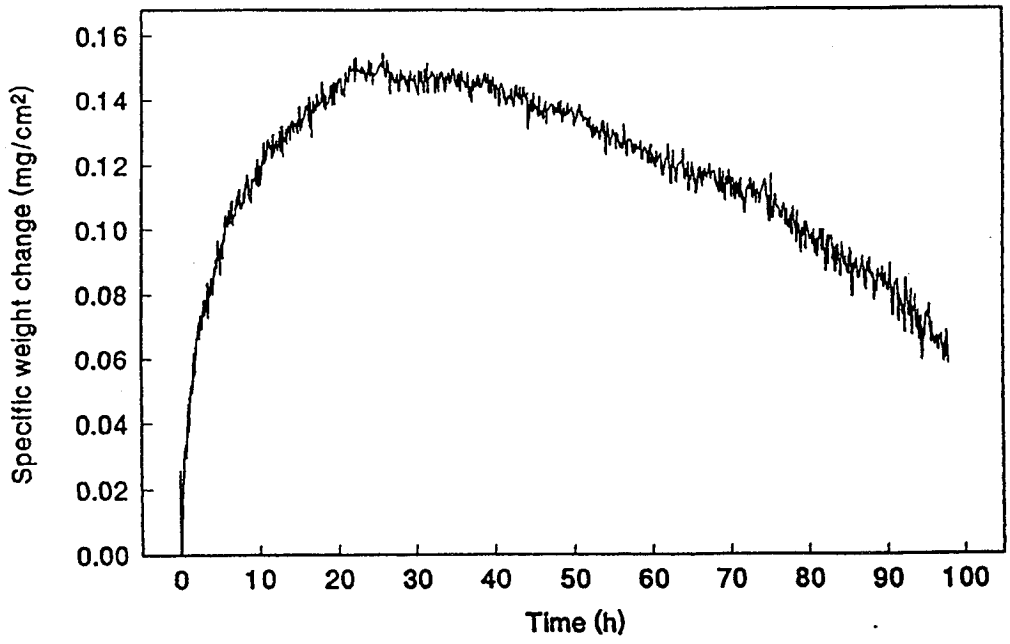

Figure 2.8 Paralinear oxidation kinetics for SiC under model lean TGA conditions (1200°C, 50%H_2O-50%O_2, 4.4 cm/s) [17].

temperatures between 1300°C and 1450°C. Figure 2.9 shows the initial weight gain progress into a linear weight loss. In this case, SiO_2 is forming as Equation 2.2, while simultaneously volatilizing to form the gaseous SiO species as Equation 2.5 and/or 2.6. Again, the partial pressure of the reacting species [$P(H_2)$, P(CO)] is important in determining P(SiO), and HPBR experiments offer a more severe environment than 1 atm TGA furnace tests.

Once again, this combination of simultaneous oxidation and linear volatilization produces overall paralinear kinetics. As with model fuel-lean conditions, paralinear oxidation kinetics are characterized by simultaneous oxide growth and volatilization. This is illustrated schematically in Figure 2.10. Initially, the overall result is weight gain as the oxidation rate is faster than the linear volatilization rate. As the oxidation rate slows down, the scale reaches an equilibrium thickness, and the net result becomes a weight loss. At this point, SiC consumption occurs at a linear rate approximated by the silica rate loss.

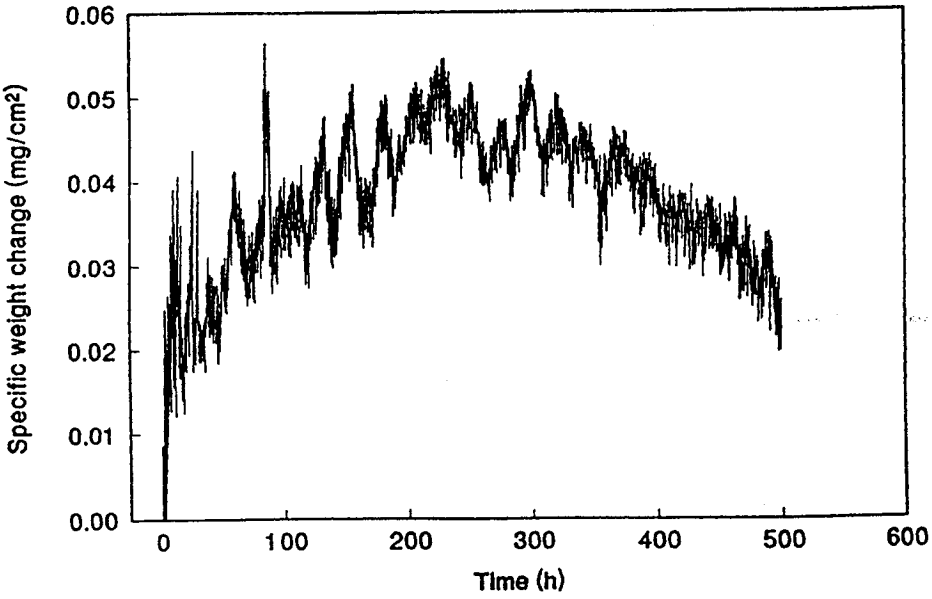

Figure 2.9 Paralinear oxidation kinetics for SiC under model rich TGA conditions (1400°C, 4%H_2-13%H_2O-10%CO-7%CO_2-bal.N_2, 0.44 cm/s) [18].

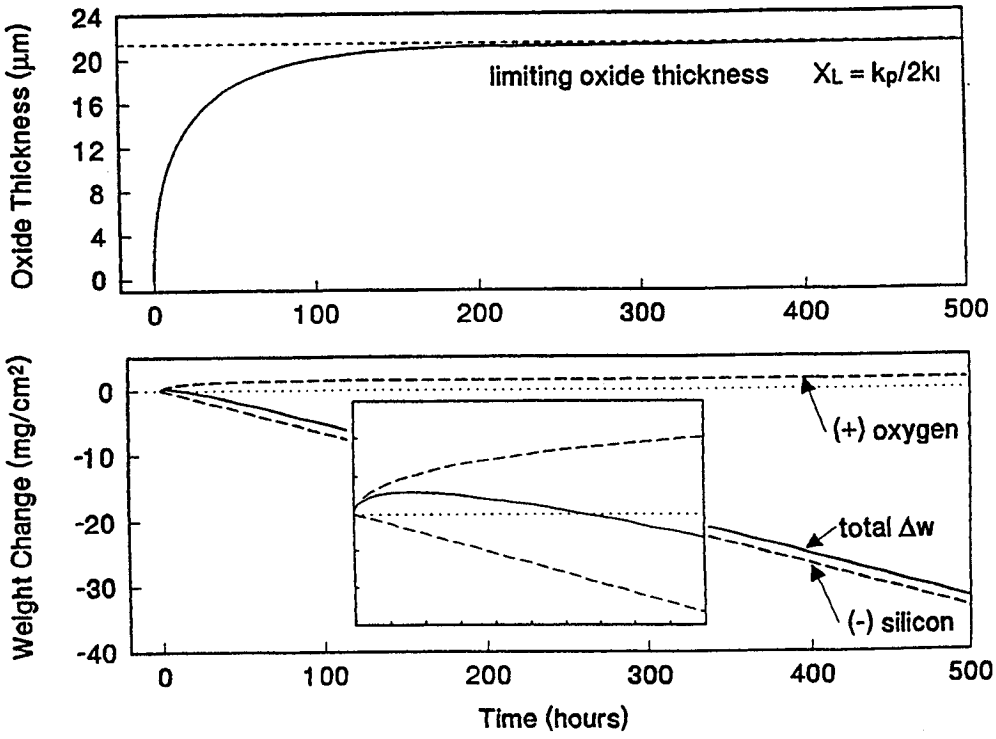

Figure 2.10 Paralinear oxidation kinetics; simultaneous oxidation and linear volatilization behaviors.

3.0 DEVELOPMENT OF EXPERIMENTAL CAPABILITIES

With the limitations of TGA studies, such as low flow rates and synthetic combustion gases, an existing pressurized burner rig at NASA LeRC was redesigned to closely simulate the environments expected in future gas turbine combustor concepts. Both hardware and operational modifications were required, resulting in the unique, world-class test facility documented in the following chapter.

3.1 Requirements

To aid theoretical chemical analyses and laboratory studies, an experimental test rig was needed to expose candidate materials to actual combustor conditions which simulate the RQL environments. To simulate the RQL combustor environment for materials test purposes, the primary parameters of interest are temperature, pressure, gas flow velocity, and most importantly, the gas composition which is set by the fuel-to-air ratio.

It has already been mentioned that liner temperatures may exceed 1650°C (2800°F). The approximate pressure for the RQL is 15 atm, with flow velocities expected to be 15-30 m/s (50-100 fps) under rich-burn operation [6]. Lean-burn operation may be closer to 90 m/s (300 fps). Other lean-burn designs may operate at pressures closer to 8 atm. The most difficult experimental requirement for the rig would be the capability for both fuel-lean and fuel-rich operation. Development of such a rig would be very costly and delay materials testing substantially. However, if an existing rig

could be modified to meet these requirements, it would expedite testing and be more economical than development of a new rig. The High Pressure Burner Rig (HPBR) in existence at LeRC was proposed as a possible facility.

The HPBR at Lewis had been used to perform a limited number of high-velocity, high-temperature environmental durability tests. However, due to its infrequent use, long-term test reliability had never been demonstrated. The rig simulates gas turbine combustor conditions by burning jet fuel and pressurized air in controlled ratios while maintaining a desired test pressure and combustion gas velocity. In addition, operation had been limited to fuel-lean mixtures only. Initial experiments in the HPBR demonstrated the feasibility of rich-burn operation at the required fuel-to-air ratios, temperatures, and pressures. However, subsequent studies concluded that 1) the fuel-air mixing was not satisfactory, 2) sufficiently low flow velocities could not be achieved, 3) the by-products of rich-burn operation were not environmentally acceptable, and 4) the use of air cooling for certain components in the test section created local hot spots under fuel-rich operation.

Modification of the HPBR to meet requirements mandated extensive redesign and introduction of innovative combustion concepts. Key efforts included the implementation of a state-of-the-art air blast fuel nozzle, removal of environmentally hazardous emissions (CO, H_2S), and the use of an inert gas for the cooling of observations windows. Materials durability

problems were another major hurdle in that conventional rig components were expected to have the durability of the advanced materials. The preliminary studies indicated that both combustor liner and sample holder durability were not satisfactory to achieve the long term testing desired.

Problems with past designs were attributed mainly to lack of proper cooling, stainless steel construction, and not utilizing thermal barrier coating (TBC) technology. Instead, high temperature superalloys, along with air and water cooling schemes, were used in designing combustor and sample holder components. Related to the other modifications, the control system of the facility was outdated. Computer control was added to ensure quality and repeatability of test capabilities and to eliminate manual data acquisition. Many of these modifications have been highlighted, along with other operational information, in a previous publication [19] but will be discussed in more detail in upcoming sections.

3.2 Current Test Rig Configuration

A schematic of the current rig configuration is shown in Figure 3.1. Combustion air enters the rig and flows over the combustor liner to provide cooling. This also preheats the air which minimizes soot formation. The air is directed through a swirler in the combustor's dome, mixed with jet fuel using an air-blast fuel nozzle. Combustion is initiated using hydrogen gas and an ignitor. Combustion products flow downstream through an optional water-cooled transition section where heat losses progressively lower the

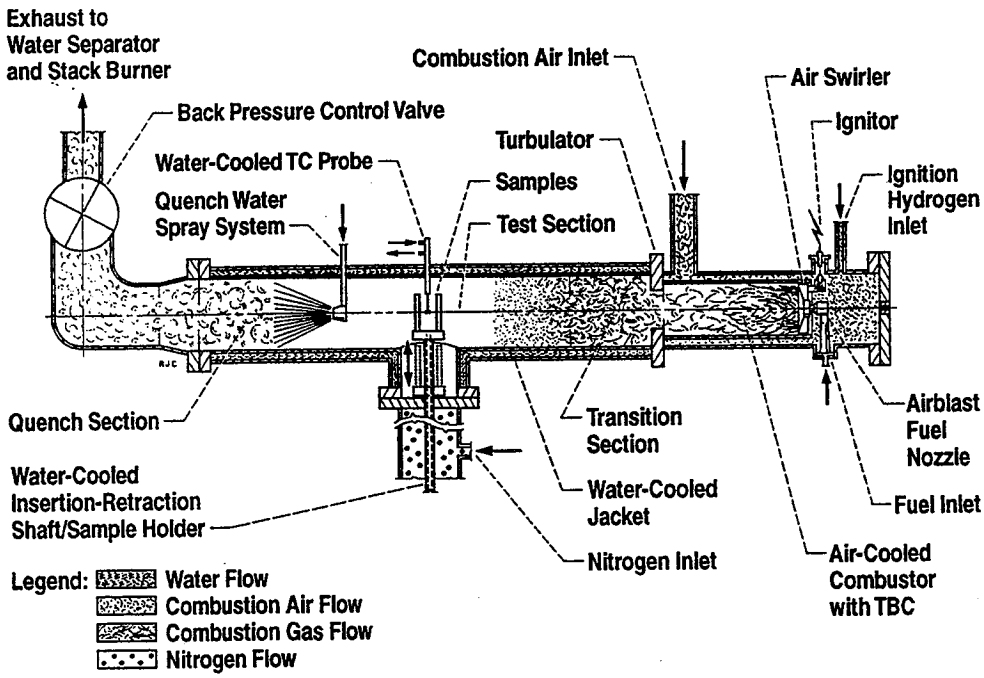

Figure 3.1 Schematic of High Pressure Burner Rig (HPBR).

downstream gas temperature. The hot gas mixture then passes through the test section and over the samples held within a fixture, and at which point the gas temperature is instantaneously measured by a water-cooled thermocouple probe. The sample holder fixture is mounted on a shaft which is inserted into the "T-section" at an angle normal to the flow.

Before exiting the rig, the combustion gases are cooled by a water spray in the quench section as they enter the back pressure control valve used to maintain the pressure of the system. The combustion gases, water, and steam pass through a solid particulate separator and natural gas stack burner before being vented to the atmosphere. This is to remove any water, soot, and certain emissions (CO, H_2S) that are not environmentally acceptable. In addition to the combustor rig the test cell contains a dedicated 400 hp compressor which delivers combustion air to the facility. The test cell layout, including the air compressor, is shown in Figure 3.2, while Figure 3.3 provides a photographic view of the test rig.

3.3 Highlight of Design Modifications

3.3.1 Combustor

The development of the existing combustor section was possibly the largest key effort in modifying the HPBR to meet testing requirements. As previously mentioned, the rig's initial configuration resulted in poor fuel-to-air mixing under fuel-rich conditions. This was evident from excessive amounts of sooting, combustion instability (frequent flameouts), and very

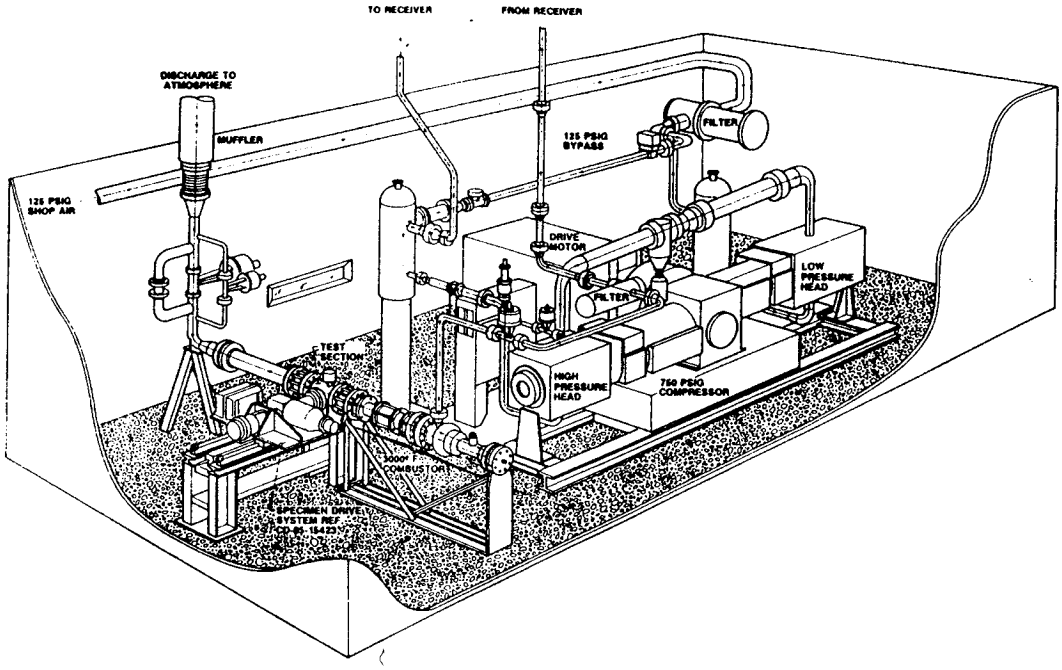

Figure 3.2 Test cell layout including 400 horsepower, high pressure air supply.

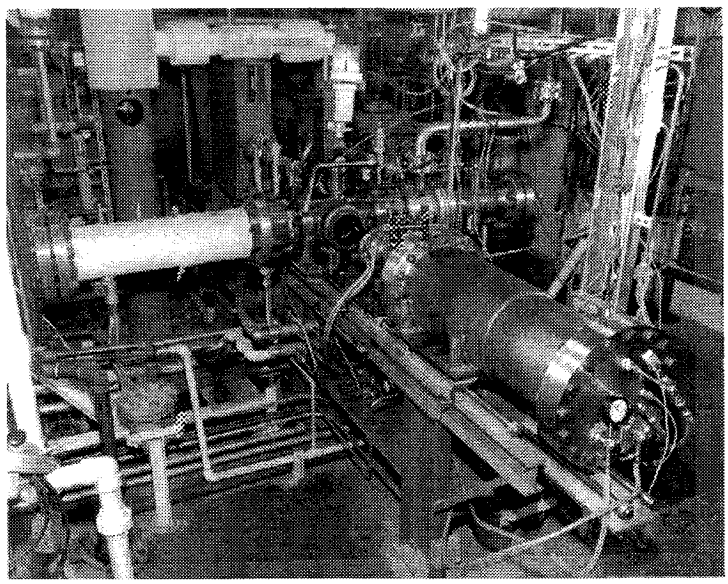

Figure 3.3 Photograph of HPBR and test cell.

nonuniform temperature profiles as mapped by the thermocouple in the test section. Through consultations with NASA, Textron[2], and University of California Irvine (UCI) combustion engineers, along with a few trial-and-error iterations, the combustor's design was optimized to the current configuration as shown in Figure 3.4.

As mentioned, combustion air enters the housing, passes through the annulus between the housing and the outside diameter of the liner, and enters the combustor dome through the swirl plate and air-blast fuel nozzle. The combustor liner, swirl plate and fuel nozzle assembly are shown in Figure 3.5. Liner durability was improved using high-temperature, superalloy material (Inconel 601[3]) and a TBC on the inside diameter. More importantly, the liner is now free to expand and contract during heating and cooling cycles. Unlike the previous design, the swirl plate is supported in the housing at three points by pins and not attached to the liner. The liner is slotted to allow for growth over the swirler and past the pins. This eliminated severe buckling encountered in earlier designs when the liner and air dome were a welded assembly, and any growth by the liner was resisted by the fuel nozzle and spark plug arrangements.

Fuel-to-air mixing was improved by changing the fuel nozzle and air

---

[2]Textron Fuel Systems, Inc., Zeeland, MI.

[3]Inconel is a tradename of Inco Alloys International, Huntington, WV.

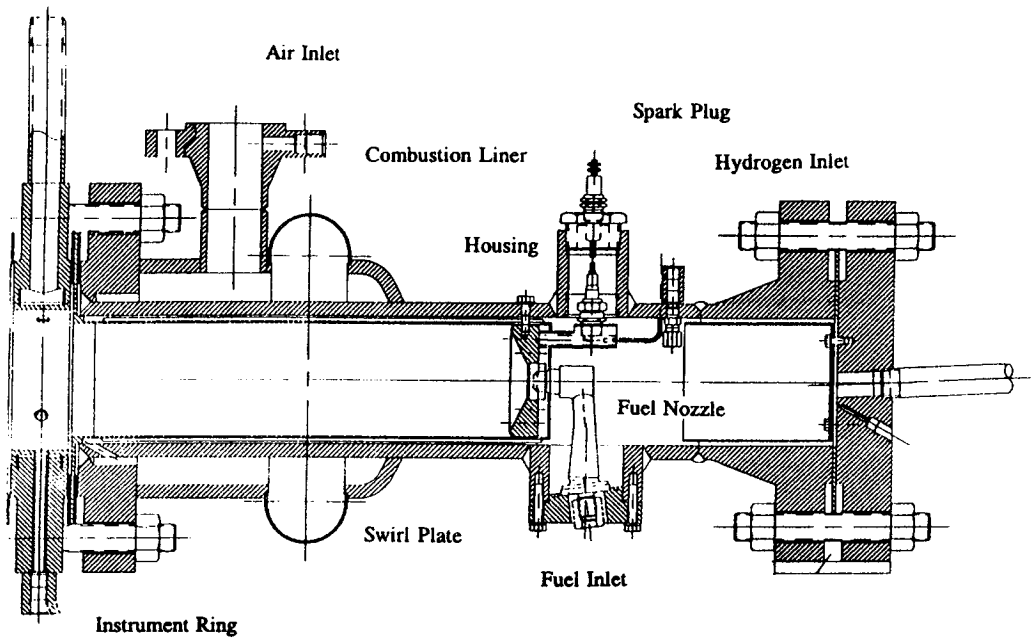

Figure 3.4 Cross section of modified HPBR combustor.

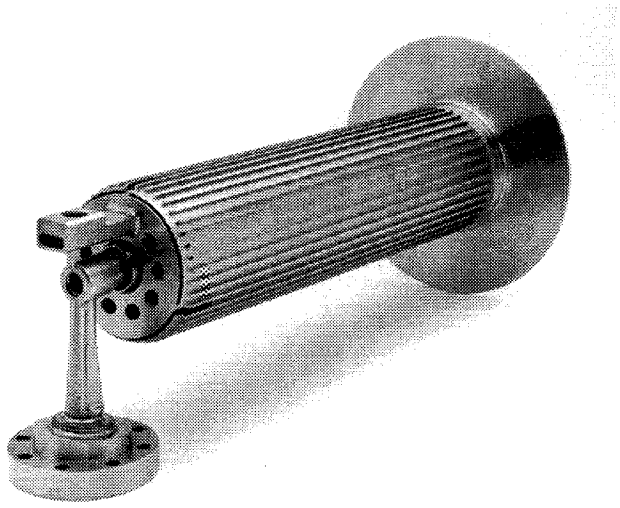

Figure 3.5 Combustor liner, swirl plate, and fuel nozzle assembly.

inlet scheme. The current design differs significantly from the original one shown in Figure 3.6. Originally, an ineffective fuel nozzle design relied on pressure to inject the fuel, and the lack of air swirl at the dome did not permit shearing of the large fuel droplets. As a result, the fuel was not properly atomized and collapsed to centerline at elevated pressures. However, the current design (Figure 3.7) uses an air-blast fuel nozzle obtained from Textron. This is the exact type used in Pratt & Whitney's 2037 gas turbine engine and considered state-of-the-art with respect to fuel atomization. The air inlet has evolved to a swirl plate which utilizes a single row of radial holes to produce air swirl (approx. 60°) with the same rotation as the fuel nozzle. In addition to the swirl angle, the geometry of the dome (conical expansion configuration) is critical in achieving proper fuel-air mixing [20]. Together, the modifications greatly improved temperature profiles, flame stability, and soot resistance as compared to that of original design.

3.3.2 Test Chamber

The next series of modifications include those in the area of the test section. To reduce the flow velocities to 15-30 m/s, a convergent flow nozzle from the original configuration was eliminated between the transition section and the test section. With the nozzle, velocities were typically 250-350 m/s (800-1200 fps). The test section in Figure 3.8 requires the use of nitrogen, as opposed to air, for cooling in two areas under rich-burn conditions. These areas were originally cooled with air which eventually

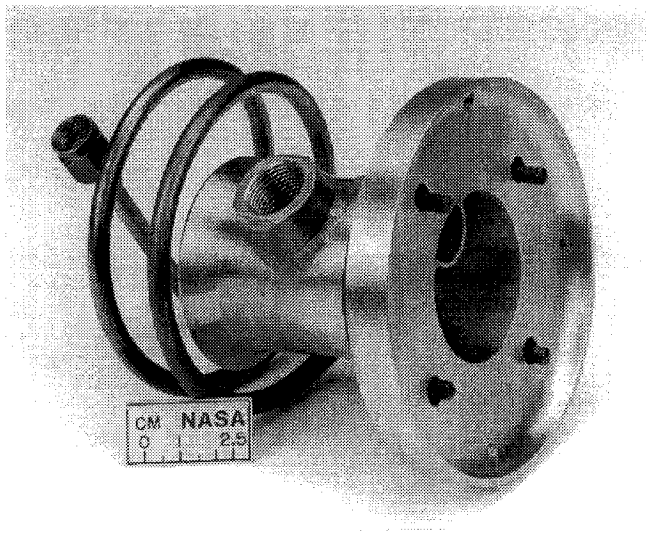

Figure 3.6 Original air inlet and fuel nozzle configuration.

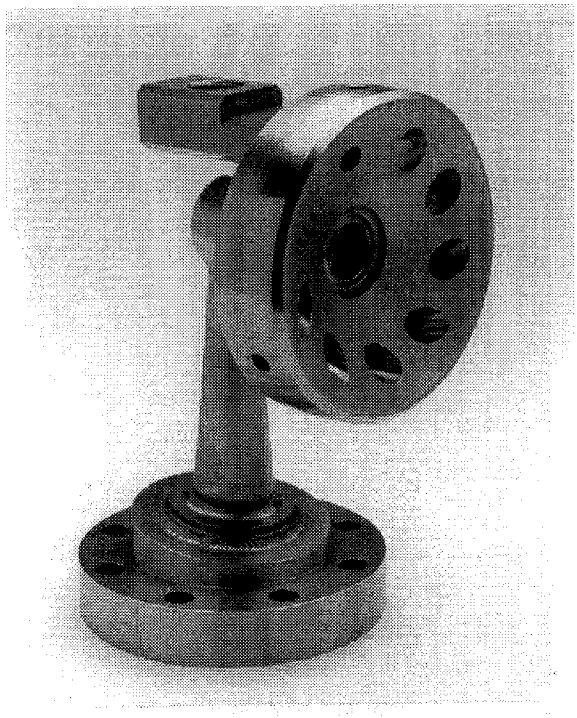

Figure 3.7 Modified fuel-air mixing scheme showing swirl plate's inlet air swirl angle, conical expansion dome, and air-blast fuel nozzle.

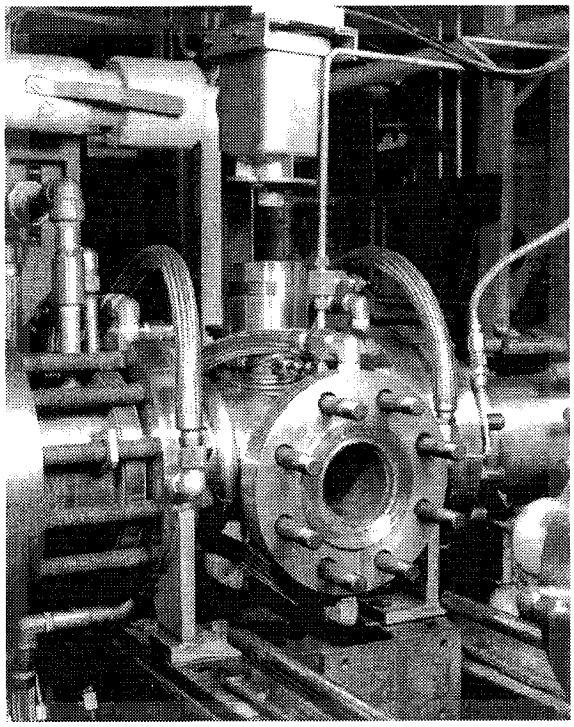

Figure 3.8 View of test section showing sample holder entrance and quartz window used for temperature measurement.

flowed into the gas path. However, under rich-burn operation, any additional air mixed into the gas path causes combustion of unburned fuel and increases temperatures. First, the observation window shown at the top of the section, which are used for temperature measurement via pyrometry, must be cooled to prevent cracking and soot deposition. Secondly, the "T-section", which houses the bearings and actuators for the shaft and holder uses a pressure seal to keep out hot gases as shown in Figure 3.9. To accomplish this the required flow rates were calculated, and a liquid nitrogen dewar and vaporizer were installed to supply nitrogen gas to the rig. One final note, both the transition and test sections were sprayed with a TBC to improve their durability.

3.3.3 Specimen Holder

Related at least in part to the modifications mentioned in the previous section was the need for a new sample holder. Without the flow nozzle, a more static environment results in higher heat transfer and puts increased demands on properly cooling the sample holder. This, coupled with the desire to minimize nitrogen use, rendered previous air-cooled holders unfeasible. As a result, the water-cooled sample holder shown in Figure 3.10 was designed, fabricated, and sprayed with a TBC. The test specimens are loosely contained in slotted superalloy grips fitted in the holder. Sample width may range from 1.3 cm (½ in.) to 2.5 cm (1 in.), with total accommodations for 4 samples in the 1.3 cm wide configuration. Because

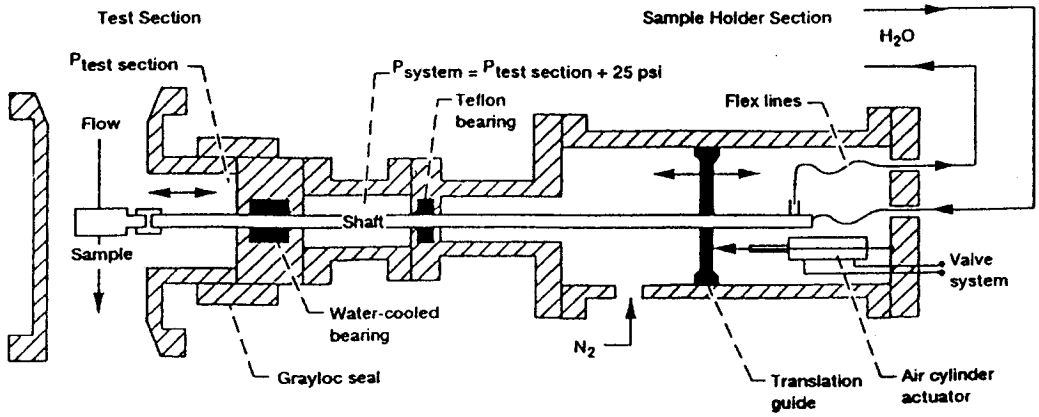

Figure 3.9 Cross section of sample holder section showing use of N_2 gas seal and insertion-retraction mechanism.

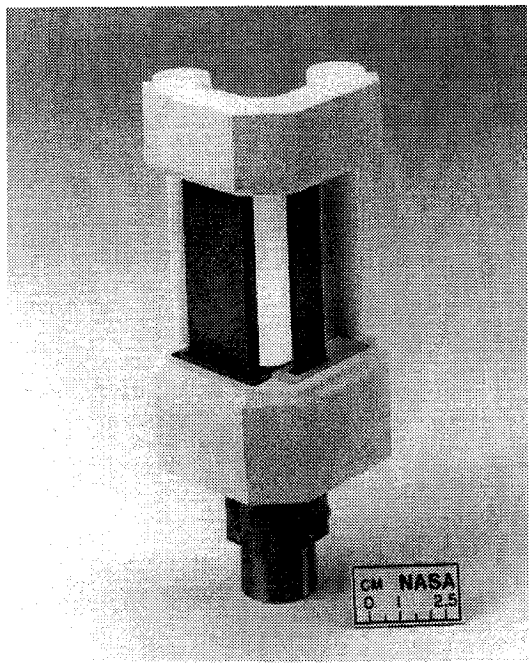

Figure 3.10 HPBR water-cooled sample holder shown with TBC coating and various size specimens.

of the holder's airfoil appearance, the two inside samples located forward and closest to the rig's gas stream centerline run hotter than the outside samples. These inside samples are referred to as leading edge (LE) samples, while the outside samples are referred to as trailing edge (TE) samples.

3.3.4 Environmental Issues

The last upgrades were to address environmental concerns under rich-burn operation. As previously mentioned, the byproducts during rich-burn operation include large amounts of soot and carbon monoxide (CO). To deal with the sooting, a water separator was installed to remove what quench water had not been converted to steam and the soot contained within. This sludge is collected in a basin and periodically pumped into the sanitation system for disposal. The hazardous emissions were a bigger challenge. Here, a large carbon monoxide fume incineration system was installed to eliminate these emissions, which also included H_2S. Shown in Appendix A, this system burns off CO using a natural gas burner to heat the effluent from the rig above the CO self-ignition temperature of 700°C.

3.4 Temperature Measurement

As mentioned, a water cooled thermocouple probe is used to measure the gas temperature in close proximity to the samples. Sample temperature is generally measured using a two color optical pyrometer which is sighted through the quartz viewport and onto the samples. Under lean-burn conditions the samples can be readily seen and their temperatures measured

with the pyrometer. Figure 3.11 shows these gas and sample temperatures (without the transition section) as a function of the fuel-to-air ratio (f/a) for monolithic CVD SiC. Note, for jet fuel the f/a is related to the equivalence ratio (ϕ) such that

$$f/a = \phi \times 0.068 \qquad (3.1)$$

where $\phi = 1$ designates the f/a where the fuel is completely burned and stoichiometric conditions exist [21]. There are significant axial and radial temperature gradients in the gas that create a temperature drop of 15-60°C (30-100°F) between the LE and TE samples. The magnitude of this temperature difference depends on pressure and velocity.

Under rich-burn conditions the sample is not visible due to intense luminosity of the flame, and sample temperatures could not be measured directly. Instead, sample temperatures are predicted during fuel-rich operation using a correlation technique. Sample temperatures measured via pyrometry in the lean-burn mode are correlated with the combustion gas temperature measured simultaneously by the test section thermocouple located directly behind the samples. These correlations (both the LE and TE positions) are shown in Figure 3.12, where a least squares fit of the data is used to obtain equations relating sample temperature to gas temperature.

These equations are used to predict the sample temperatures in the rich-burn mode, however some assumptions must be made. In predicting these sample temperatures, it is assumed that the relationship between the

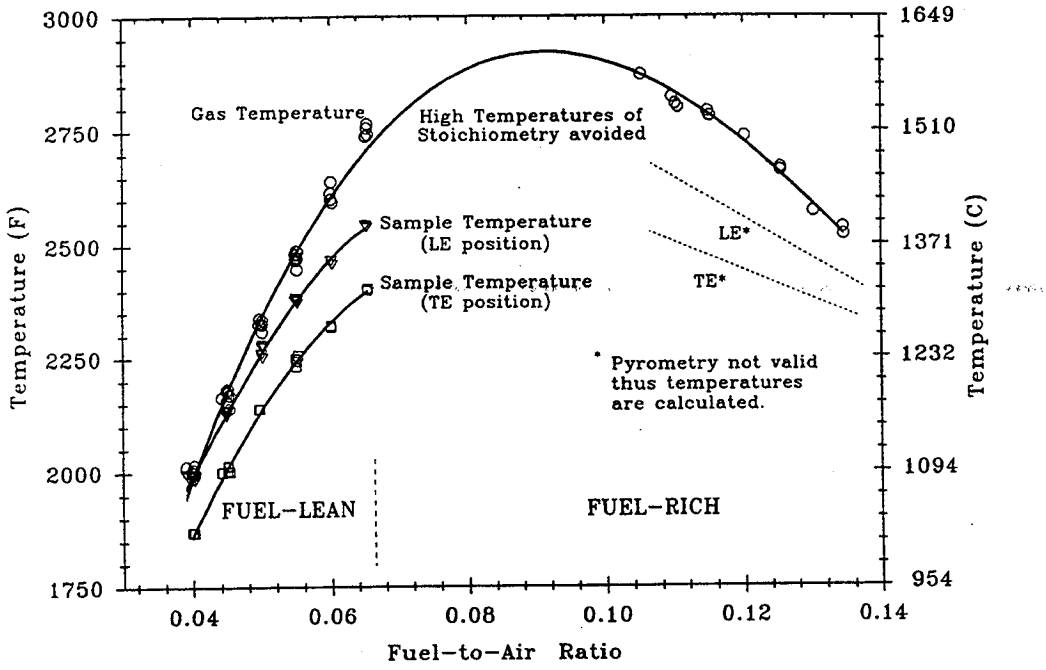

Figure 3.11 Gas and both sample (LE and TE) temperatures as a function of fuel-to-air ratio.

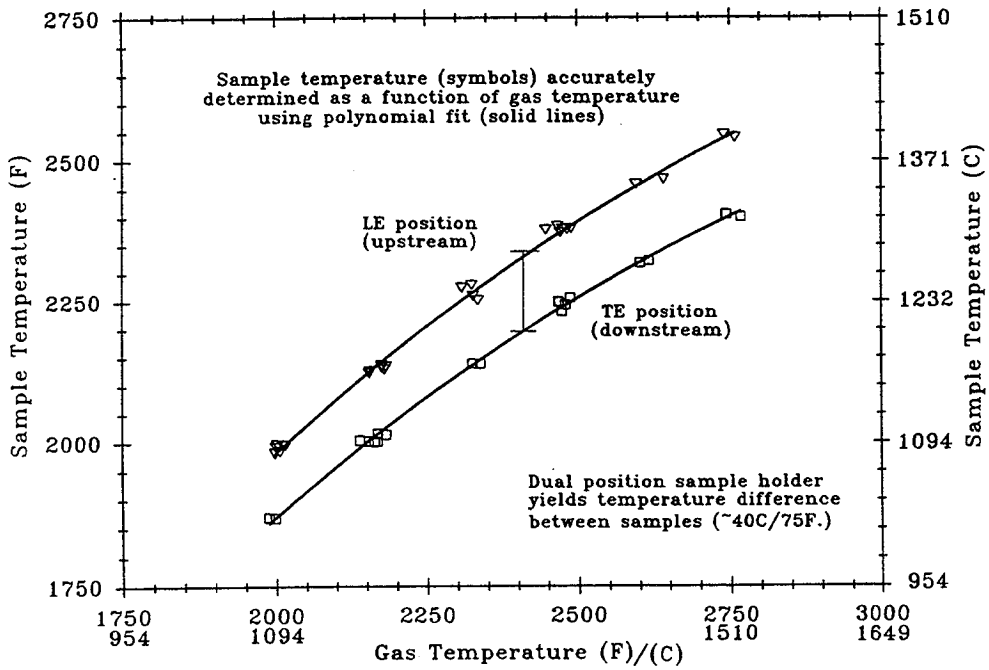

Figure 3.12 Correlation between gas and sample temperatures.

sample temperature and the gas temperature, measured in the lean-mode, still holds during rich-burn operations. This assumption appears reasonable since the mass air flow, pressure, and gas velocity, which have all been verified experimentally to influence the calibrations, are held constant. The difference in combustion products between the lean and rich modes is expected to make little difference in heat transfer. Not surprisingly, the calibration curves are also strongly dependent on the sample material. Therefore, a separate calibration curve is generated for each material, test condition, and sample position tested.

3.5 Operating Specifications

The test capabilities developed encompass a wide range of operating conditions. The standard mode of operation is to control the fuel-to-air ratio (f/a) for a fixed air flow rate (m_a) and fixed test pressure (P_t). The rig typically operates at air flows set between 0.45 and 0.68 kg/sec (1.0-1.5 lbm/sec). This range is restricted by the requirement to provide adequate cooling to the combustor liner over the complete operating range of the combustor which has broad stability limits. Operation at slightly higher air flows is possible for lean-burn conditions, however the CO fume incinerator is limited to approximately 0.6 kg/sec under rich-burn conditions. Combustion can be maintained over equivalence ratios of approximately $\phi = 0.3\text{-}0.9$ and $\phi = 1.5\text{-}2.0$ for lean-burn and rich-burn conditions, respectively. Much of the region around stoichiometric conditions ($\phi = 1.0$-

1.5) is avoided to minimize rig durability problems resulting from the high temperatures associated with this region. Equivalence ratios in excess of 2.0 are avoided because of sooting. The system pressure can be varied between 4 and 15 atm, but caution is required at the higher pressures. Here, fuel-air mixing is compromised by a reduced pressure drop across the dome swirler, and the durability of the combustor liner and sooting can become a problem. To correct these problems, air flow is generally increased to raise the pressure drop across the combustor.

The resultant gas temperature (T_g), sample temperatures (T_s), and gas velocity (V_g) are dependant variables, fixed by the selected f/a, m_a, and P_t. If the f/a and P_t selected are such that moderate combustion temperatures are attained, the rig can run with m_a as low as 0.23 kg/sec (0.5 lbm/sec) and still have sufficient cooling for the combustor liner. Gas velocity (V_g) is a calculated quantity derived using the ideal gas law ($pv = nRT$):

$$Vg = 1.85(m_a \cdot T_g/P_t) \qquad (3.2)$$

where the constant $1.85 = fn[R, A_{test}]$ and A_{test} is the area of the test section. Velocity is calculated at the point of temperature measurement. In the current configuration, gas velocity typically ranges from 9 to 27 m/s (30-90 ft/sec).

4.0 EXPERIMENTAL

A pressurized burner rig at NASA LeRC was used to perform the high-temperature, environmental durability tests. Monolithic SiC coupons were exposed to both fuel-rich and fuel-lean simulated combustor conditions. Recession of the SiC was measured using both weight loss and direct thickness measurement techniques.

4.1 Test Material

The primary material chosen for the experiments was dense, high purity CVD SiC[4] to avoid any complications due to porosity, sintering aids, or non-stoichiometric Si and C. The material is highly pure (99.999 percent), containing < 100 ppm of each Be and Cu. The composition is slightly silicon rich ($Si_{1.03}$) and contains no voids (0 percent porosity). Although SiC ceramic-matrix composites (CMCs) are a more likely combustor material, the monolithic material was chosen to eliminate weight loss associated with composite architecture and fiber coatings.

In addition to the CVD material, Hexoloy SiC[5] was supplemented in limited cases (25%) due to material availability. This sintered α-SiC contains some free carbon, resulting in a slightly carbon-rich composition [22]. Hexoloy is also highly dense and very pure, containing the trace elements

---

[4]Morton International, Inc., Woburn, MA; chemical vapor deposition process.

[5]Carborundum Structural Ceramics Division, Niagara Falls, NY; sintered or reaction-bonded process.

Al(~0.09 wt.%), Fe(~0.03 wt.%), and B(~0.36 wt.%). In most cases, the Hexoloy samples were tested along side CVD material and resulted in weight changes that differed only by 1-3% of those obtained on CVD material. As a result, the two materials were not treated separately in the analysis. All samples were machined to the dimensions 7.6 cm (3 in.) x 1.3 cm (½ in.) x 0.3 cm (⅛ in.) as shown in Figure 4.1 to utilize the 4 sample, multi-temperature level configuration.

4.2 Test Parameters

Sample materials were exposed to both the lean-burn and rich-burn conditions similar to those used in both conventional lean-burn and RQL combustor operation. For all tests the operating parameters included a fixed mass air flow rate (m_a) and test pressure (P_t). Nearly one half of the data was obtained under standard conditions of $m_a = 0.45$ kg/sec (1.0 lbm/sec) and $P_t = 6$-6.3 atmospheres. Fuel-lean mixtures ($\phi < 1$) were varied between 0.76 and 0.94, producing sample temperatures (T_s) that ranged 1200-1450°C (2200-2650°F). Fuel-rich mixtures ($\phi > 1$) were varied between 1.54 and 1.97, and using the correlation technique produced $T_s = 1225$-1450°C (2250-2650°F).

Figure 4.2 shows the temperatures for the combustion gas, LE samples, and TE samples as a function of the fuel-to-air ratio. The fuel-lean and fuel-rich regions actually studied are shown as shaded areas. In addition, the reduced temperature curve using the water-cooled transition

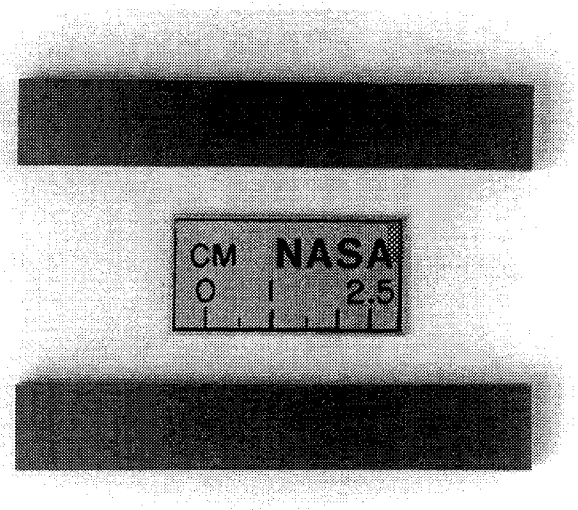

Figure 4.1 HPBR CVD SiC specimens (7.6 cm x 1.3 cm x 0.3 cm).

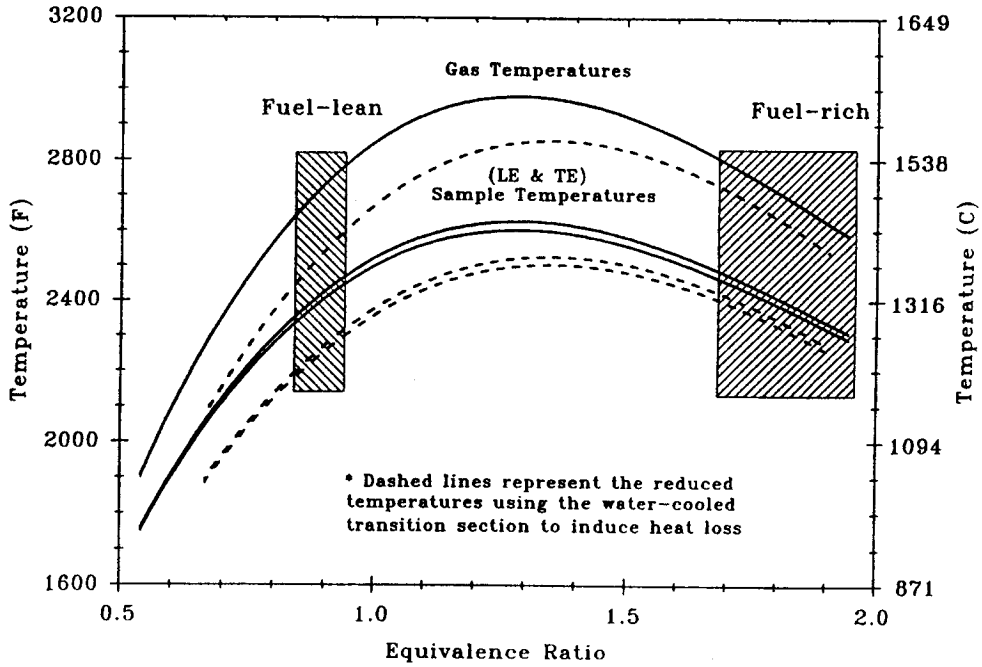

Figure 4.2 Available HPBR experimental temperature ranges (gas, LE, and TE). Those fuel-air mixtures actually studied are noted.

section is also illustrated. As a result, there are four possible sample temperatures for any given ϕ.

Gas velocity is a dependent variable which is fixed by m_a, P_t, and T_g. For standard conditions, gas velocity varied directly with T_g (as m_a and P_t were constant throughout a test) and ranged 18-24 m/s (60-80 fps). However, a subsequent number of different test pressures were also used over the same temperature range by modulating the exit gas valve. Restriction of the valve increased back pressures up to 10 atm rich-burn and 15 atm lean-burn, but simultaneously reduced velocities down to about 15 and 10 m/s (50 and 30 fps), respectively. Here, mass air flow rates were increased (to 1.2-1.5 lbm/sec) to ensure proper fuel-to-air mixing in the combustor. Under rich-burn conditions, coking of the combustor can occur, which causes damage as carbon chunks are shed and strike the samples. Conversely, opening the exit valve decreased pressures down to 4 atm for rich-burn and 5 atm for lean-burn, with resultant gas velocities increasing to near 27 m/s (90 fps). Exposure times ranged between 20 and 100 hrs. Longer times were required at lower temperatures and pressures to allow acceptable measurement of smaller recession rates.

Experimental testing was performed in three phases. In Phase I, standard conditions were used to define temperature effects by varying sample temperature. In Phase II, operating pressures, as well as mass air flow rates, were varied to define pressure effects. These first two phases

included both lean-burn and rich-burn matrices. In Phase III, sample orientation was varied under lean-burn conditions to determine any effects of gas impingement angle. A parametric summary (including T_s, P_t, V_g, ϕ, and number of data points) of the complete, 3-phase test matrix is given in Table 4.1.

Table 4.1 - Summary of experimental test parameters.

	T_s (°C)	P_t (atm)	V_g (m/s)	ϕ	no. Pts
Phase 1-Rich	1225-1450	6-6.3	18-24	1.69-1.97	19
Lean	1200-1450	6-6.3	20-23	0.87-0.94	12
Phase 2-Rich	1240-1420	4-10	15-27	1.54-1.88	15
Lean	1225-1435	5-15	10-20	0.78-0.88	12
Phase 3-Lean	1295-1420	10	18-19	0.76-0.87	6

4.3 Recession Measurements

The experimental data included both weight change measurement and direct surface thickness measurement. Measurements were generally taken at 8-16 hr intervals during routine inspection of the test section and sample holder components. For weight change measurement, the specimens were weighed on a digital scale to 0.001 gms and normalized to surface area (cm^2). The hot area was assumed to include the entire sample except for the ⅛ in. ends held in the specimen holder grips. Thickness measurements of the

sample were taken using vernier calipers. The sensitivity of the calipers was 0.0013 cm (0.0005 in.). Measurements were taken at three cross-sections (-½ in., 0, + ½ in.) and averaged. Recession was generally uniform at each of the three cross-sections measured along the length of the samples. In calculating material loss rates, the weight change measurements typically showed less regression error than direct thickness measurements and are therefore regarded as the more accurate recession measurement technique for pure, monolithic SiC.

5.0 RESULTS

5.1 Temperature Effects

In this Phase I of experimental testing, the temperature dependence of SiC recession was determined. Tests were conducted under standard conditions, where pressure and velocity were held relatively constant for both fuel-rich and fuel-lean mixtures.

5.1.1 Fuel-Rich Mixtures

Weight change and thickness measurements were plotted versus time, generating the two respective curves for each of 19 test points. Figures 5.1 and 5.2 show a series of four such curves for weight change and thickness, respectively. For both figures, each curve represents a different test point (ie. sample temperature). Only 4 of the 19 tests are shown for clarity, however nearly the entire temperature range of the study is represented with these four curves. These plots initially indicated two major points: 1) there is weight loss and surface recession of the SiC material which is linear with increasing exposure time; and 2) a strong temperature dependence exists producing increasing weight loss and surface recession with an increase in temperature.

In regards to the temperature dependence using Figure 5.2, the maximum thickness decrease actually measured was approximately 125 μm in nearly 100 hours at 1385°C. This is compared to a 25 μm thickness decrease measured at 1252°C for the same 100 hours. From the slope of

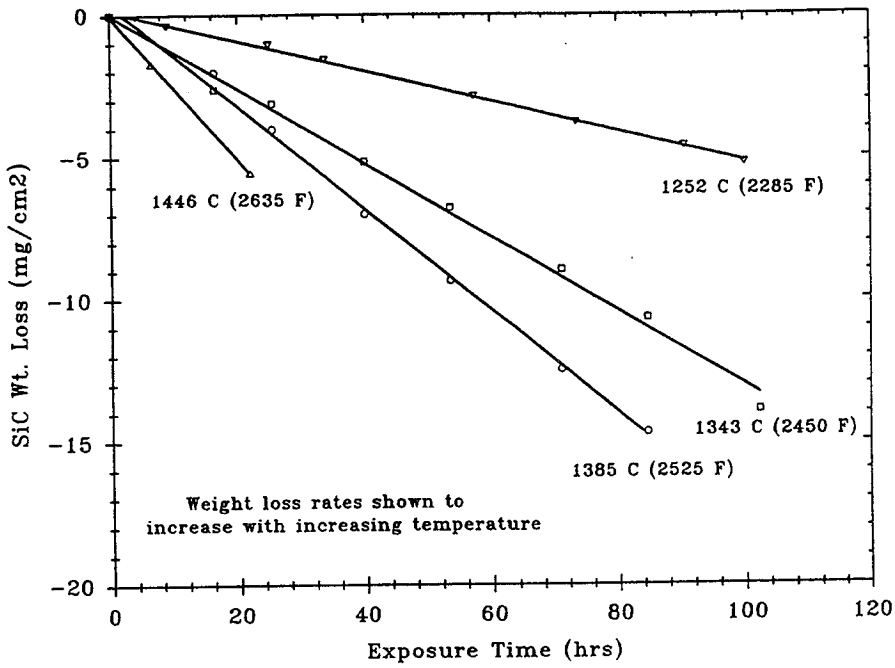

Figure 5.1 Weight loss vs time for various temperatures under standard rich-burn operating conditions ($P_t = 6.3$ atm, $V_g = 18\text{-}20$ m/s).

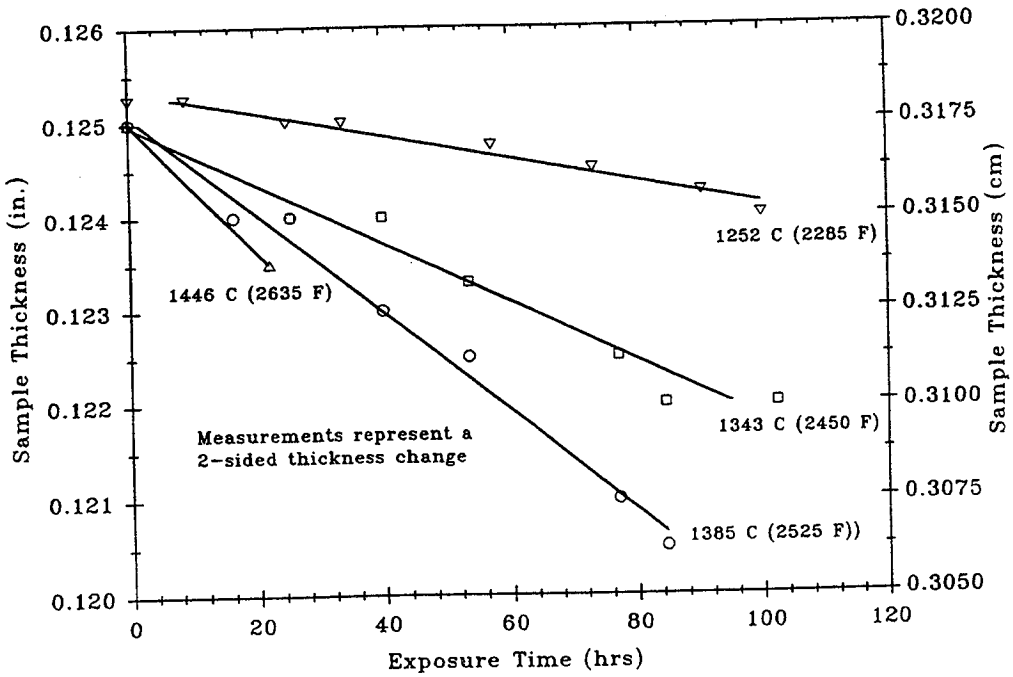

Figure 5.2 Thickness change vs time for various temperatures under standard rich-burn conditions ($P_t = 6.3$ atm, $V_g = 18\text{-}20$ m/s).

each curve in Figures 5.1 and 5.2, a rate loss constant (k_l) for both weight change (mg/cm^2-hr) and surface recession (μm/hr) can be obtained. These rates are shown in Table 5.1 along with corresponding temperatures. Note, the rates obtained for surface recession represent the total decrease in thickness from both major sides combined.

Table 5.1 - Linear recession rates (k_l) obtained from weight loss (mg/cm^2-hr) and direct 2-sided thickness (μm/hr) measurements.

Temperature (°C)	Wt. Loss (mg/cm^2-hr)	Recession (μm/hr)
1252	-5.20×10^{-2}	-0.31
1343	-1.30×10^{-1}	-0.80
1385	-1.79×10^{-1}	-1.33
1446	-2.52×10^{-1}	-1.74

Plotting the log of k_l as a function of 1/T, an Arrhenius-type curve was generated for both weight loss and surface recession (only 15 pts. available). Both curves are plotted in Figure 5.3. The solid line represents the recession rates, which have been factored (halved) to represent recession per side. This allows comparison with an acceptable material loss rate is 254 μm (10 mils) per 18,000 hrs (1.41×10^{-2} μm/side-hr). At 1300°C (2375°F), the material loss rate obtained is over an order of magnitude higher. This is confirmed by the weight loss curve (represented by the dashed line). As before, the rate at 1300°C is over an order of magnitude

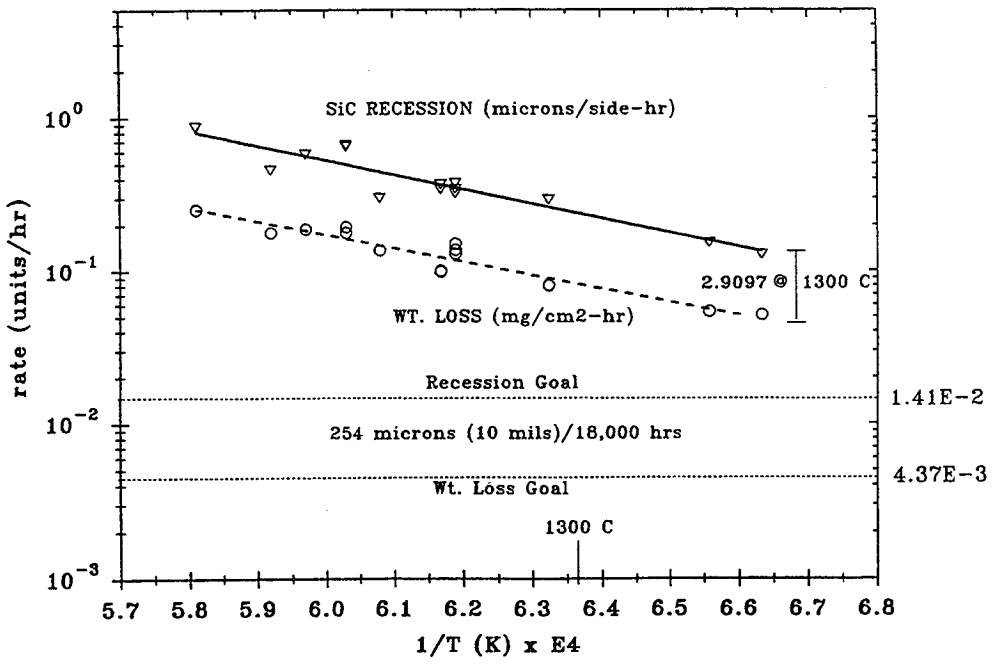

Figure 5.3 SiC weight loss and surface recession for standard rich-burn conditions (T_s = 1225-1450°C, P_t = 6-6.3 atm, V_g = 18-24 m/s).

higher than the acceptable loss rate (4.37×10^{-3} mg/cm^2-hr), also shown below. The weight loss goal was calculated from the acceptable material loss rate using the density of CVD SiC (3.21 g/cm^3). The conversion factor of SiC weight loss (mg/cm^2) to surface recession (μm) is 3.115. In good agreement, a factor of 2.910 was measured experimentally at 1300°C.

The loss rates were fit by the Arrhenius equation, defined as $\text{Rate} = A \cdot \exp(-\Delta E^*/kT)$ for thermally activated processes [23]. This resulted in the following equations for SiC material loss:

$$\Delta X(\mu m) = 2.515 \times 10^5 \cdot [10^{-181 kJ/mol(2.3)R(T°C+273)}] \cdot t \qquad \textbf{(5.1)}$$

$$\Delta X(\mu m) = 1.245 \times 10^5 \cdot [10^{-171 kJ/mol(2.3)R(T°C+273)}] \cdot t \qquad \textbf{(5.2)}$$

where Equations 5.1 and 5.2 predict the recessions from direct thickness measurements and converted weight changes, respectively. The linear regression of the data results in reasonably good fits, with typical deviation limits represented by R^2 values of 0.94 and 0.97 for Equations 5.1 and 5.2. ΔX gives the SiC recession (μm/side) as a function of sample temperature in degrees Celsius (T°C) and exposure time in hours (t). As expected, the two slopes in Figure 5.3 are similar, providing two separate measures of the activation energy (ΔE). The slopes of Figure 5.3 (-9460 and -8937) were multiplied by the gas constant (R), where R is the product of Boltzmann's constant (k) and Avogadro's number, to obtain $\Delta E = 181$ kJ/mol and $\Delta E = 171$ kJ/mol for Equations 5.1 and 5.2, respectively. The factor 2.3 is also required to account for the use of Log_{10}, where $\ln(x) = 2.3\text{Log}_{10}(x)$.

At 1300°C, Equation 5.1 predicts 2.44×10^{-1} μm/side-hr and Equation 5.2 predicts 2.59×10^{-1} μm/side-hr. These rates are in good agreement, and as stated, both exceed the acceptable limit of 1.41×10^{-2} by over an order of magnitude. Using the weight loss equation for material loss, Table 5.2 lists the predicted recession for various times (extrapolated up to 10,000h) and temperatures. Here, the acceptable limit of 254 μm (10 mils) in 18,000 hrs for maximum allowable material loss is exceeded for temperatures >1200°C after only 1000 hrs, and for all temperatures at 10,000 hrs, as highlighted (underlined bold type) in Table 5.2.

Table 5.2 - Predicted recession (μm/side) for fuel-rich mixtures at standard conditions ($P_t = 6\text{-}6.3$ atm, $V_g = 18\text{-}24$ m/s).

Time (hrs)	1200°C	1300°C	1400°C
1	0.107	0.259	0.567
10	1.067	2.594	5.669
100	10.67	25.94	56.69
1,000	106.7	**259.4**	**566.9**
10,000	**1067.**	**2594.**	**5669.**

5.1.2 Fuel-Lean Mixtures

Although the primary focus of Phase I was on rich-burn conditions, a comparable number of tests (12) were conducted in an attempt to map lean-burn recession over the same range of standard conditions

(temperature, pressure, and velocity). Note, from this point onward recession is discussed using the converted weight loss technique (as opposed to direct thickness measurements). This is due to the smaller scatter in weight loss data, which is directly related in part to equipment sensitivity. In addition, an increased test duration was required to obtain accurate rates from thickness measurements.

Figure 5.4 shows k_l from the weight loss data in an Arrhenius plot for the lean-burn tests as compared to the rich-burn data. Although still significant, the recession under lean-burn conditions is not as severe. Less temperature dependence is also exhibited than under rich-burn conditions. The Arrhenius relation for fuel-lean mixtures becomes:

$$\Delta X(\mu m) = 5.35 \times 10^{2} \cdot [10^{-111 kJ/mol/(2.3)R(T°C+273)}] \cdot t \qquad \textbf{(5.3)}$$

where Equation 5.3 also gives the SiC recession in μm/side from converted weight changes. Again, the linear regression is a good fit of the data ($R^2 = 0.96$), and ΔX is given in terms of sample temperature ($T_{°C}$) and exposure hours (t). In Figure 5.4, the slope of the lean-burn curve is -5799, which translates into an activation energy of 111 kJ/mol.

Equation 5.3 predicts a recession of 1.10×10^{-1} μm/side-hr at 1300°C (2375°F), clearly indicating that lean-burn recession rates also exceed the acceptable limit of 1.41×10^{-2}. In this case, the limit is exceeded by nearly an order of magnitude. Figure 5.4 also suggests that possibly, due to the difference in temperature dependence, lean-burn recession will be greater

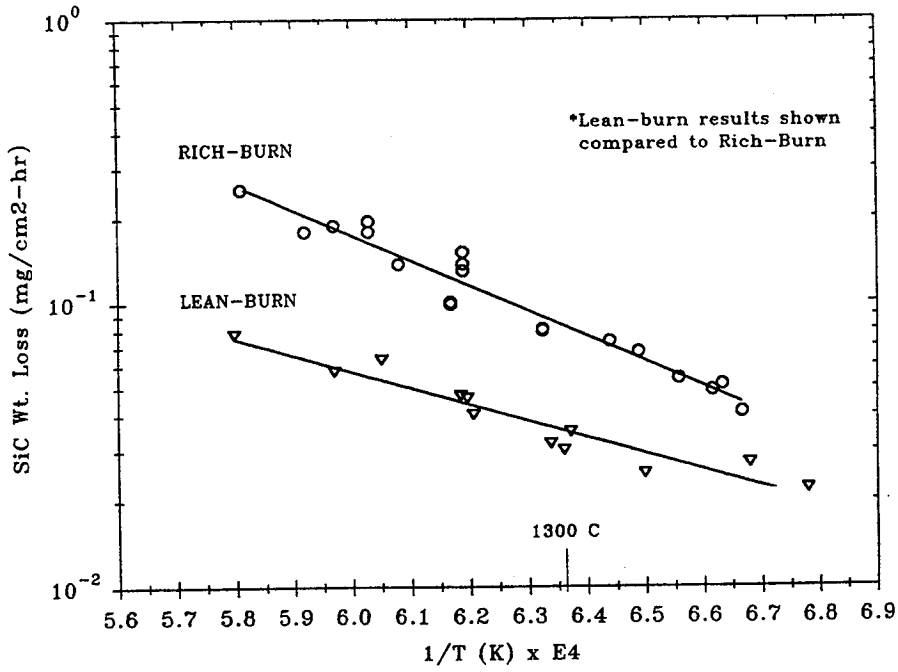

Figure 5.4 SiC weight loss under standard lean-burn conditions (T_s = 1200-1450°C, P_t = 6-6.3 atm, V_g = 20-23 m/s) compared to rich-burn results.

than rich-burn recession at lower temperatures. However, this could not be determined due to the rig's limitations. Table 5.3 shows some typical recession values predicted for fuel-lean mixtures. Here, the unacceptable material loss (shown again in underlined bold type) occurs at all noted temperatures after 10,000 hrs. Again, this is clearly short of the 18,000 hour life required.

Table 5.3 - Predicted recession (μm/side) for fuel-lean mixtures at standard conditions (P_t = 6-6.3 atm, V_g = 20-23 m/s).

Time (hrs)	1200°C	1300°C	1400°C
1	0.062	0.110	0.183
10	0.619	1.101	1.829
100	6.187	11.01	18.29
1,000	61.87	110.1	182.9
10,000	**618.7**	**1101.**	**1829.**

5.2 Pressure Effects

In Phase II, the effect of pressure on SiC recession was determined for both rich-burn and lean-burn conditions. In addition to temperature, pressure and air flow rates were varied, and results are compared to those obtained during Phase I under standard conditions.

5.2.1 Deviation From Standard Operating Conditions

The expected pressure of the RQL combustor has been published as

15 atm. For all tests using standard conditions, the pressures were representative but slightly lower (6-6.3 atm) than actual conditions. Any increase or decrease of material loss rates due to pressure changes must be determined. However, there are limitations to the HPBR in achieving this. Figure 5.5 shows the effect of increased test pressure on rig performance.

Increased pressure raises the combustion gas temperature (as well as sample temperature) for a given ϕ and poses potential rig durability problems. As previously mentioned, air flows must be increased to maintain proper fuel-to-air mixing within the dome region of the rig's combustor. As a result, velocity is also affected. Increased temperature and air flow raises the velocity, while the higher pressures counter to lower the velocity. In addition, temperature is less sensitive to fuel-to-air changes under rich-burn conditions. This limits the temperature range available at the higher pressures. These concerns have limited the number of high pressure test points that which were performed at any given nonstandard condition.

5.2.2 Fuel-Lean Mixtures

Figure 5.6 demonstrates the result of increased pressure on the material loss rates for a series of lean-burn tests conducted at an average sample temperature of 1327°C (2423°F). Again, the lean-burn volatile species is expected to be $Si(OH)_4$ formed as Equation 2.4. Here, weight loss is also seen to increase with pressure for 4 tests that range in pressure from 5 to 15 atm. Resulting flow velocities were typically 20 m/s (65 fps), with

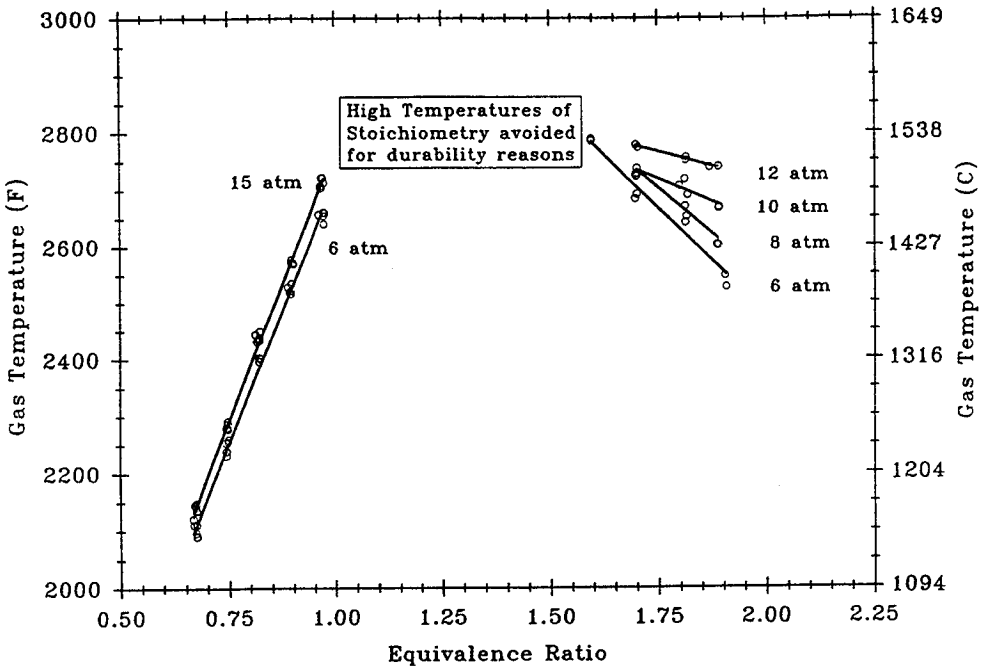

Figure 5.5 The effect of increased operating pressure on HPBR gas temperatures.

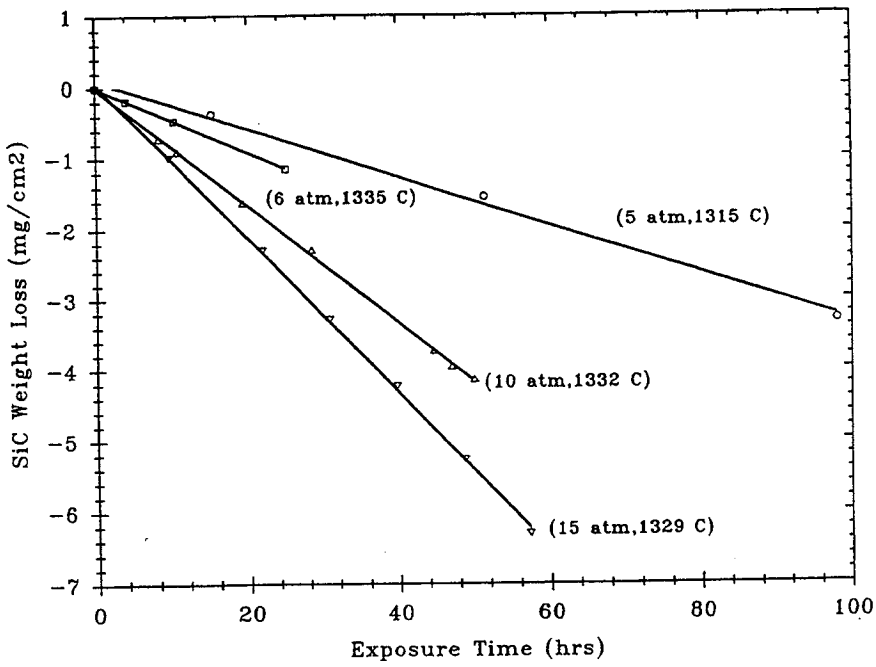

Figure 5.6 Pressure effects (5-15 atm) on SiC weight loss for typical 1327°C (2423°F) lean-burn test conditions.

the exception of the 15 atm test, which had a relatively low velocity of 10 m/s (32 fps). This low velocity was achieved early in the studies before air flow rates were being increased at high pressure. However, combustor durability was compromised. In this case, carbon buildup at low velocity was not a concern due to the fuel-lean mixture of the gases.

Illustrated in the familiar Arrhenius-type format, Figure 5.7 shows the k_l obtained from weight losses for 12 high pressure lean-burn test points as compared to previously noted low pressure results. At 10 atm, the SiC recession is greater than that under standard 6-6.3 atm conditions by a near equal amount for the entire temperature range. In comparison, the resulting flow velocities of the 10 atm tests are slightly lower, but the linear regression of the data is very similar. The 10 atm linear regression curve fit ($R^2 = 0.98$) generates an activation energy of 124 kJ/mol as compared with 111 kJ/mol for the 6 atm data. Although not mapped over all temperatures, limited tests near 1315°C (2400°F) for 5 and 15 atm confirm the same pressure effect. The 5 atm data appears to be proportional to the 6 and 10 atm data. However, the 15 atm data lies close to the 10 atm data. In fact, the relatively low gas velocity supports a velocity effect as well.

5.2.3 Fuel-Rich Mixtures

Next, the effect of pressure under rich-burn conditions was investigated. Here, rig limitations were a bigger concern than under lean-burn conditions. At high pressure, obtaining low temperature data was

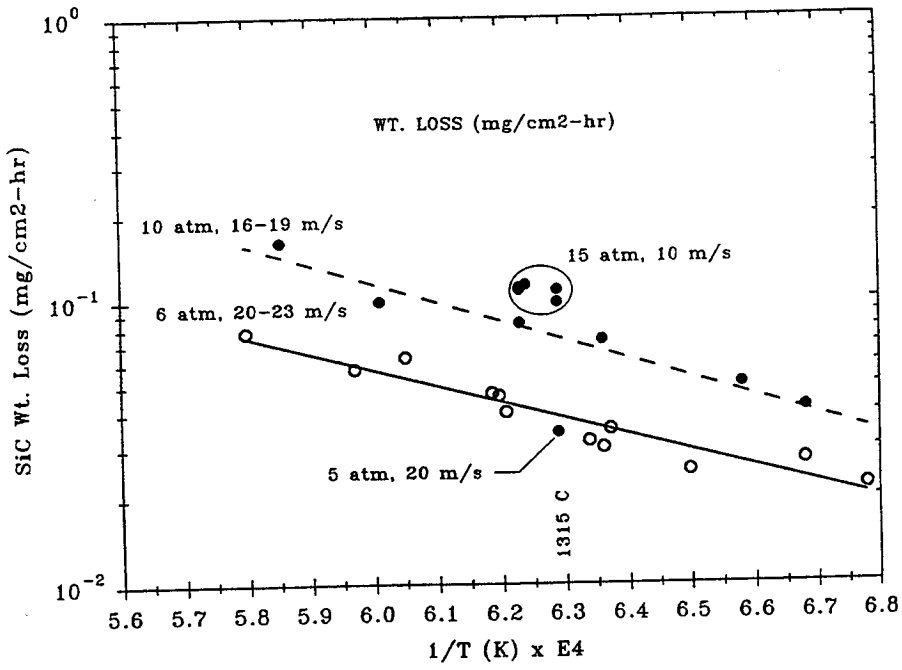

Figure 5.7 HPBR SiC recession results under lean-burn conditions (T_s = 1200-1450°C, P_t = 5-15 atm, V_g = 10-23 m/s).

difficult due to potential carbon buildup. For proper fuel-air mixing, increased pressure requires increased air flow, which raises the temperature. To counter this, fuel flow can be increased but may lead to carbon buildup.

Figure 5.8 shows the Arrhenius plot for 15 test points, ranging from 4 to 10 atm, compared to those obtained under standard conditions. As with lean-burn, the k_l measured from weight losses increased with pressure. The resulting gas velocities were as high as 27 m/s (87 fps) and as low as 15 m/s (49 fps) for 4 and 10 atm, respectively. Again, the effects seem proportional except at 10 atm, where the data appears to overlap the 8 atm data, again possibly due to differences in velocity. Although the data is limited, linear regressions were performed for 4 ($R^2 = 0.99$) and 8 ($R^2 = 0.98$) atm, yielding activation energies of 144 and 149 kJ/mol, respectively. By comparison, the data at standard conditions (6-6.3 atm) resulted in an activation energy 171kJ/mol.

5.3 Impingement Angle Effects

In Phase III, the effect of gas impingement angle on SiC recession is explored by varying sample orientation in the HPBR. In a real combustor, the flow of the combustion gases is parallel to the liner material, as opposed to the HPBR where the impingement angle is 45°. Therefore, an experiment was performed to address the concern for the severity of recession as a function of impingement angle. As shown in Figure 5.9, rotating the sample holder 45° brings one sample position of the holder to 0° and the other to

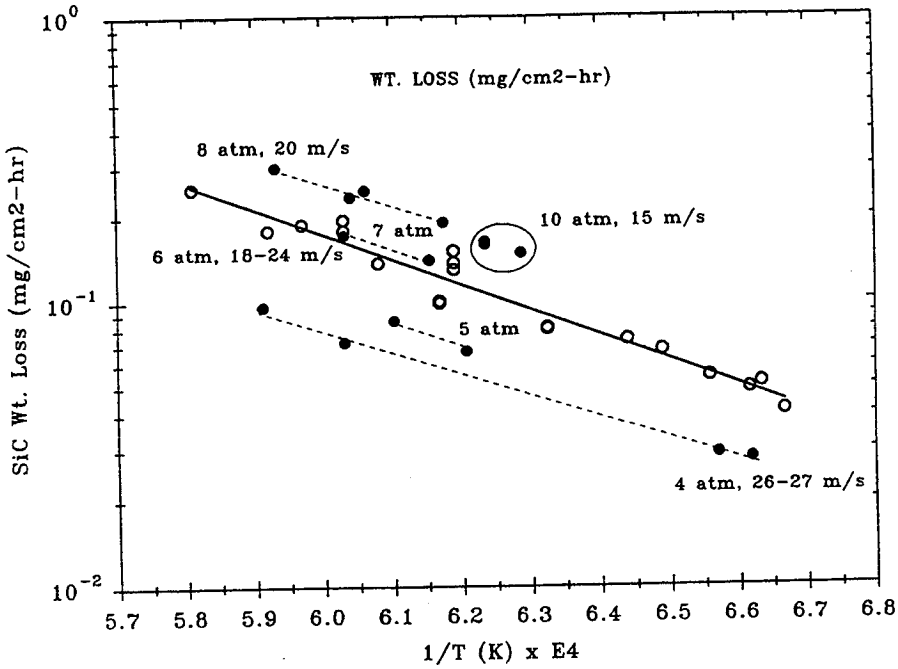

Figure 5.8 HPBR SiC recession results under rich-burn conditions (T_s = 1225-1450°C, P_t = 4-10 atm, V_g = 15-27 m/s).

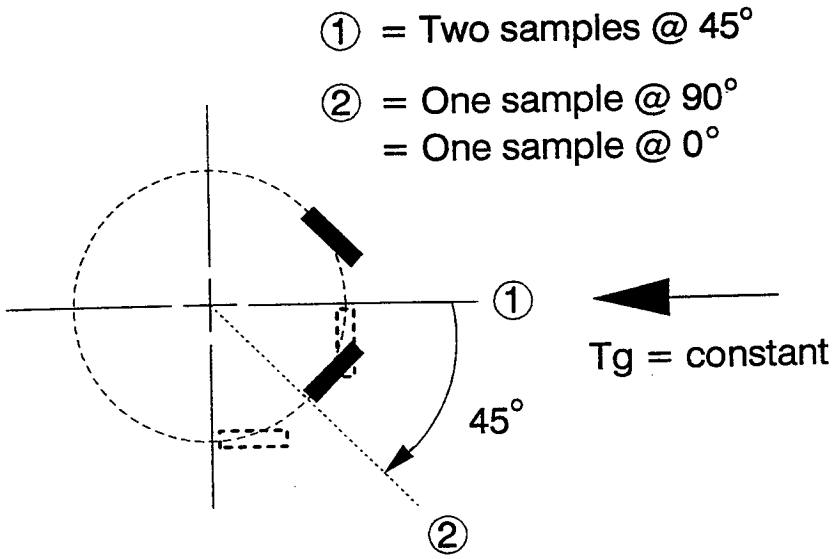

Figure 5.9 Sample orientation illustration showing typical 45° arrangement rotated to 0°/90° impingement angles.

90°. Recession rates were measured for two samples before and after rotation, as well as rotation at a second test temperature. This experiment was run under lean-burn conditions at 10 atm and 18-19 m/s (60-62 fps). The results are shown below in Table 5.4.

Table 5.4 - Lean-burn recession rates at varying gas impingement angles.

Imp. Angle	T_s (°F)	V_g (m/s)	Wt. Loss (mg/cm^2-hr)
0°	1292	18	0.055
45°	1339	18	0.093
45°	1339	18	0.082
90°	1308	18	0.062
0°	1404	19	0.125
90°	1418	19	0.125

The recession rates at 0° and 90° show little difference from those at 45° for both temperatures tested. For the first set of test conditions, the 45° rates are higher because this setup keeps the samples closest to both the centerline of the gas flow and the combustor exit causing exposure to a higher temperature. The comparisons are shown graphically in Figure 5.10. Here, all the points fall nearly on top of the previously reported 10 atm lean-burn regression line. Therefore, it is concluded that no significant effect of specimen orientation exists for the relatively low velocities studied.

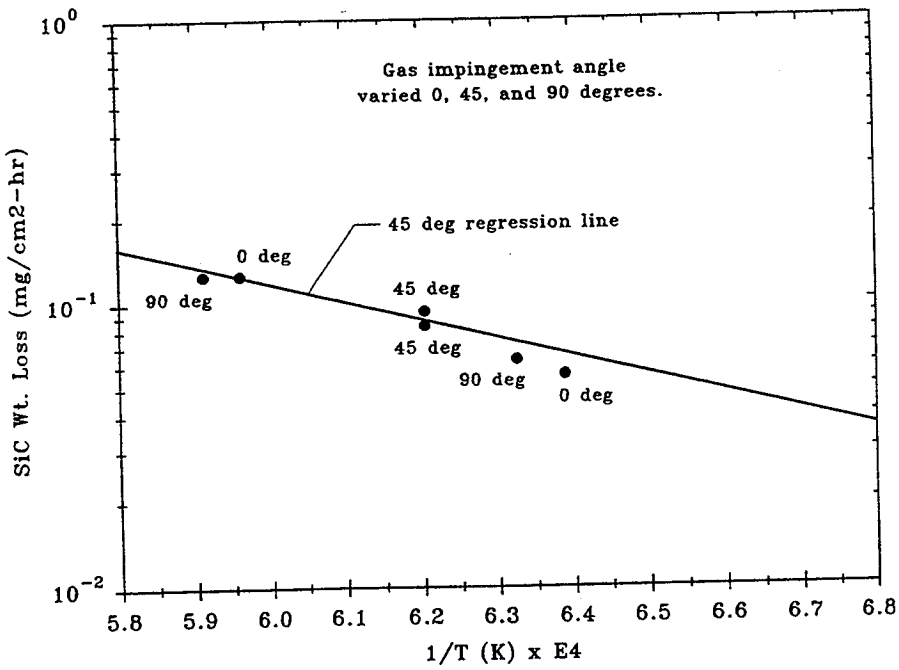

Figure 5.10 Results of impingement angle study (1290-1420°C, 10 atm, 18-19 m/s) indicate no effects on volatility.

5.4 Surface Appearance and Microstructure

Using SEM (scanning electron microscopy), the surface appearance of a HPBR sample was documented after 102.3 hours of rich-burn exposure. The test conditions included $T_s = 1343°C$, $P_t = 6.3$ atm, and $V_g = 19$ m/s, which resulted in a relatively high weight loss rate of 0.130 mg/cm^2-hr. Both the frontside and backside of the sample were examined, whereby the frontside is defined as the face on which the gas impinges directly. The sample appears visually undamaged, with an overall matte appearance suggestive of a thin oxide scale. Besides Si and O, only traces of Zr, most likely from TBC-coated hardware in the test section, and Ca were found.

Figure 5.11 shows the backside of the sample (100X), indicating some type of pits in the SiC. These pits appear uniform and are present on the frontside as well, as shown in figure 5.12. At 1000X and slightly higher magnification, the pitting appears, at least in part, to be created from spalling that occurred on the SiC surface. In Figure 5.13, a spalled region of SiO_2 from the backside of the sample uncovers oxide "ridges" in the basin, formed as oxygen penetrates cracks in the scale. This is known to be cristobalite cracking, a polymorphic transformation which occurs in SiO_2 [24]. The cracking is the result of a high volume change (shrinkage) during the transformation from high temperature β-cristobalite to low temperature α-cristobalite. Figure 5.14 (5000X) clearly shows the cracks and surface of the SiO_2, a tunneled structure which has been referred to as "popcorn".

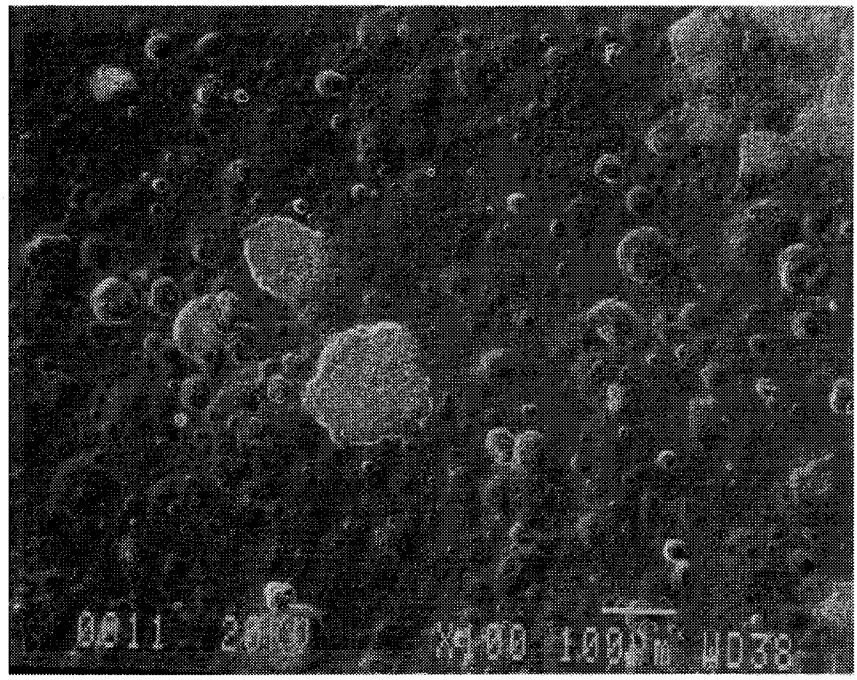

Figure 5.11 Backside of sample (100X magnification), showing evidence of surface pitting.

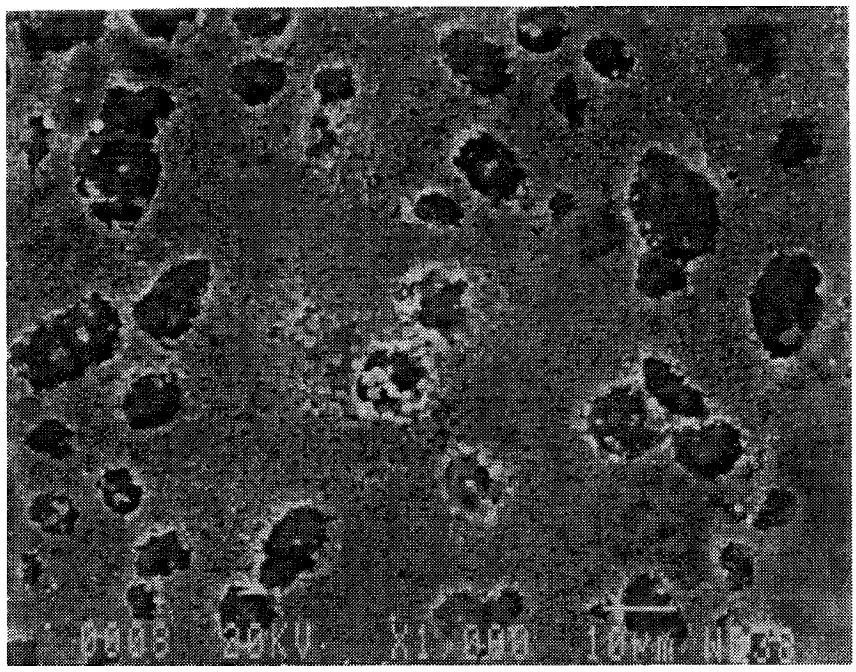

Figure 5.12 Higher magnification (1000X) of the frontside suggests potential spalling in addition to pitting.

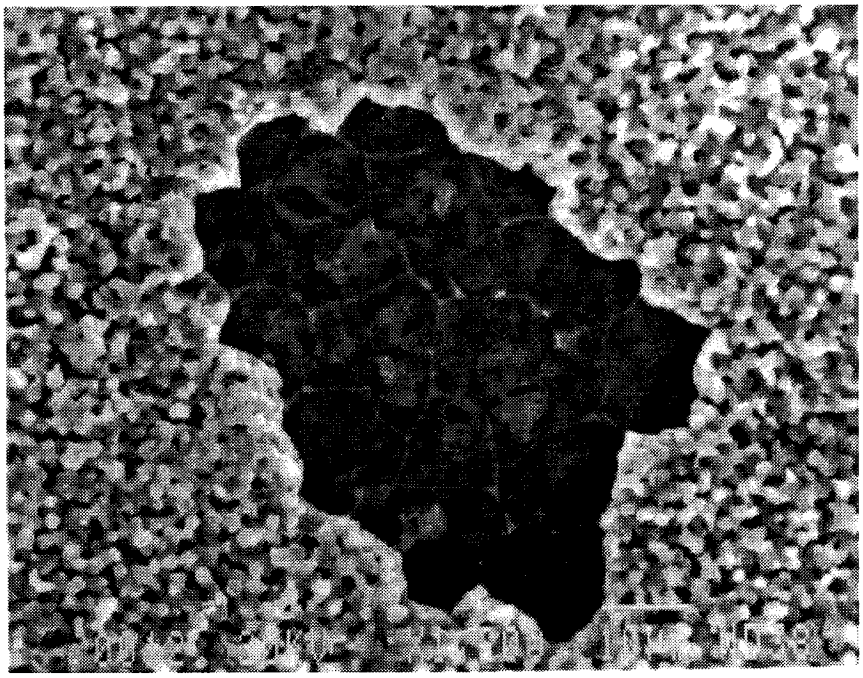

Figure 5.13 Spalled SiO_2 (1200X) uncovers oxide "ridges" in the basin, formed as oxygen penetrates cristobalite cracks in the scale.

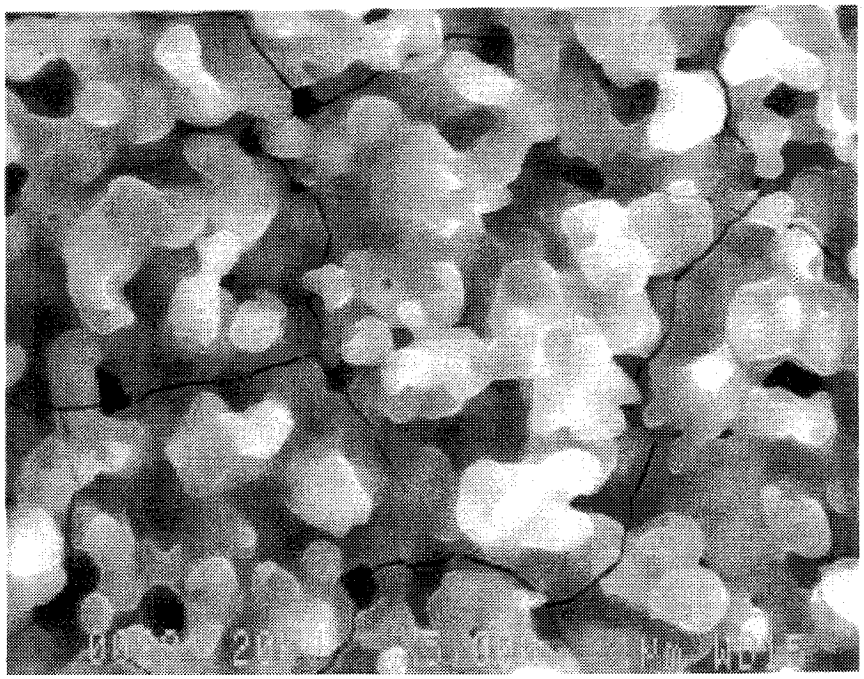

Figure 5.14 High magnification (5000X) of cristobalite cracks and SiO_2 surface. Tunneled structure has a "popcorn" appearance.

6.0 DISCUSSION AND ANALYSIS OF RESULTS

Surface recession has been well characterized in actual rich-burn and lean-burn HPBR tests and is compared to both theoretical results and furnace tests performed in model rich and lean gas mixtures. The exact volatile species under fuel-rich conditions has not yet been verified, leaving theoretical modeling in question. Therefore, a precise parametric dependence was developed to predict SiC recession for untested combustor conditions. Although the fuel-lean chemical model appears to be better understood, a parametric dependence has also been developed. Results indicate significant surface recession of SiC occurs after only 1000 hours of exposure under some typical combustor conditions.

6.1 Thermodynamic Considerations

The discussion and analysis of SiC recession under combustor conditions centers around the chemical reactions between the SiO_2 scales formed and the combustion gases flowing over the material. As mentioned, equilibrium calculations predict that the chemical makeup of the combustion gases under rich-burn conditions ($\phi = 1.5$) are $6H_2$-$12H_2O$-$12CO$-$5CO_2$-bal.N_2. SiO(g) is predicted to result from the reaction of SiO_2 with H_2. By comparison, lean-burn conditions ($\phi = 0.5$) are calculated to form combustion gases containing $10O_2$-$8H_2O$-$7CO_2$-bal.N_2 at equilibrium. Here, reaction of SiO_2 with water vapor is predicted to form $Si(OH)_4$(g). $Si(OH)_4$ formation is also possible in the rich regime. The partial pressure for these

two volatile products is defined by the equilibrium constants given in Equations 6.1 and 6.2 for SiO and $Si(OH)_4$, respectively:

$$k_{eq} = P_{SiO} \cdot P_{H2O}/(a_{SiO2} \cdot P_{H2}) \quad \textbf{(6.1)}$$

$$k_{eq} = P_{Si(OH)4}/(a_{SiO2}) \cdot (P_{H2O})^2 \quad \textbf{(6.2)}$$

where a_{SiO2} is the activity of silica. The k_{eq} vary as $\exp(-\Delta G_f/RT)$, where ΔG_f is the free energy change of each reaction. The volatilization rate, or flux (J), is defined by the boundary layer equation for transport of the vapor species from a flat plate into a moving gas with laminar flow [6,16]:

$$J = 0.664\ (Re)^{1/2}(Sc)^{1/4}D\rho v/L \quad \textbf{(6.3)}$$

where Re = Reynolds number and Sc = Schmidt number. The other variables in Equation 6.3 include concentration (ρ), velocity (v), and interdiffusion coefficient (D) of the gaseous species. The characteristic length of the sample (L) is also significant. A schematic which illustrates the SiO_2 volatility and SiC recession process is shown in Figure 6.1. As a result, the net flux at a fixed temperature of each gaseous species varies as indicated by Equations 6.4 and 6.5 for SiO and $Si(OH)_4$, respectively.

$$J_{SiO} = f\ [v^{1/2} \cdot P_{H2}/P_{H2O} \cdot (P_{total})^{1/2}] \quad \textbf{(6.4)}$$

$$J_{Si(OH)4} = f\ [v^{1/2} \cdot (P_{H2O})^2/(P_{total})^{1/2}] \quad \textbf{(6.5)}$$

These expressions become very useful as parametric scaling factors used for extrapolating results between TGA, HPBR, and HSCT conditions.

6.2 Comparison of Theoretical, TGA, and HPBR Results

The results of the entire TGA test matrix performed by Fox under

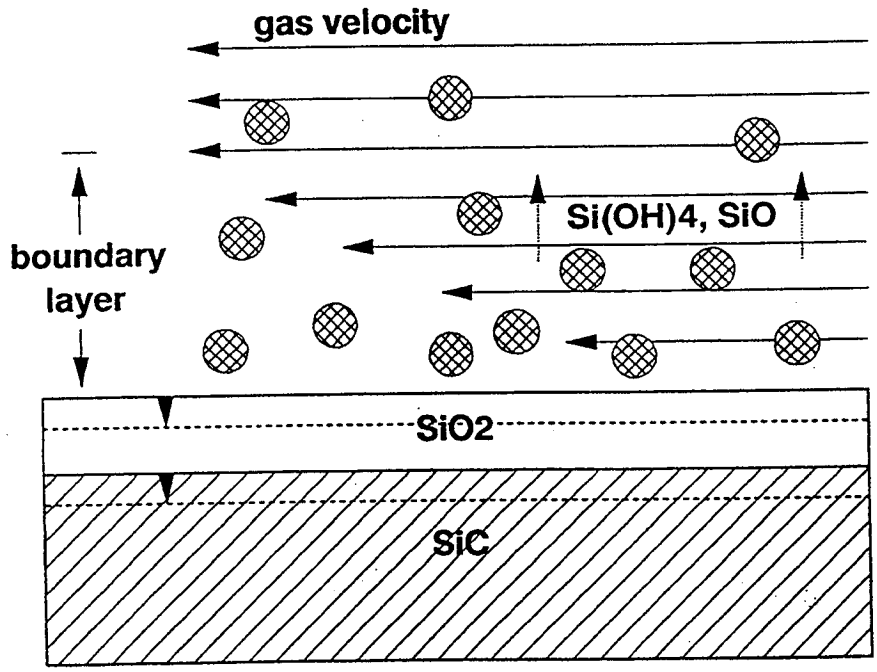

Figure 6.1 Schematic of SiO_2 volatility and SiC recession.

model rich combustion gas are summarized in Figure 6.2 [18]. The log of the linear weight loss rate (mg/cm^2-hr) is plotted as a function of 1/T (K^{-1}). Here, a strong temperature dependence is observed. Data was gathered from both a computer fit to paralinear behavior and direct measurements from pre-oxidized CVD SiC samples. Initially, the boundary layer rates predicted were lower than those measured, but the two curves converged when corrections were made to account for differences between the boundary layer thickness and furnace tube dimensions.

Results from both techniques are in good agreement and together produced an activation energy (450 kJ/mol), as well as loss rates, nearly equal to that predicted (520 kJ/mol) from the thermodynamic data and boundary layer equation for SiO formation. The agreement confirms that SiO is the correct chemical model and must be the volatile species present in the furnace. Note, these rates are more than three orders of magnitude below the maximum SiO volatility which is predicted by the Langmir equation [6] for evaporation into a vacuum.

In the TGA studies by Opila [17] under model lean conditions, experiments were run by adding 0%, 10%, and 50% H_2O to pure O_2. There was no difference between dry O_2 and 10%H_2O-90%O_2, but paralinear behavior was observed in the presence of 50% water vapor for reasons previously discussed. The results for the 50%H_2O-50%O_2 studies are summarized in Figure 6.3 in an Arrhenius plot of log recession rate as a

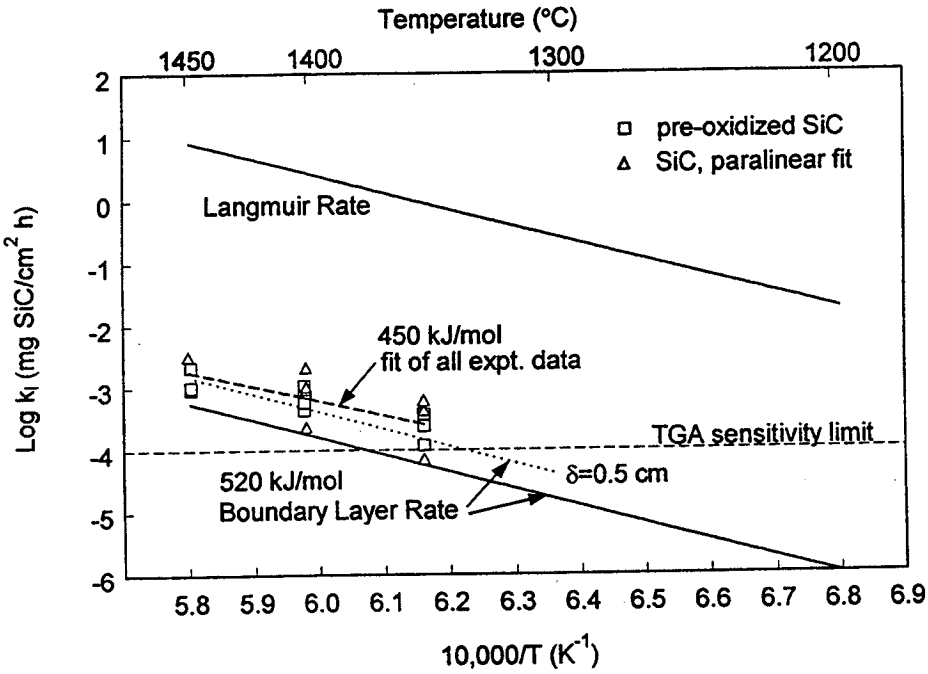

Figure 6.2 TGA weight loss for CVD SiC in model rich conditions (1 atm, 4%H_2-13%H_2O-10%CO-7%CO_2-66%N_2, 0.44 cm/s) [18].

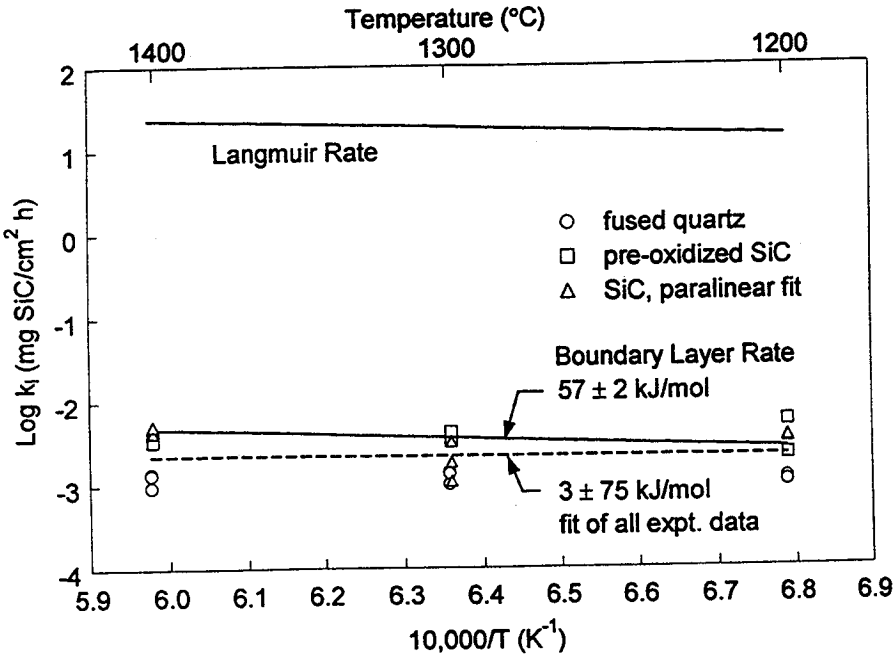

Figure 6.3 TGA weight loss for CVD SiC in model lean conditions (1 atm, 50%H_2O-50%O_2, 4.4 cm/s) [17].

function of 1/T. Here, results obtained from pre-oxidized SiC, bulk SiO_2, and a computer paralinear fit to CVD SiC oxidation are again very similar.

As with fuel-rich gas mixtures, the TGA furnace data agrees quite well with the proposed chemical model, in this case $Si(OH)_4$. The temperature dependence is not significant and appears to be slightly different than theoretical. By comparison, the activation energies are 3 and 57 kJ/mol for the respective measured and theoretical values. However, the magnitude of recession is quite close to that predicted from thermodynamic data and the boundary layer equation. Again, the Langmir rate is significantly higher than experimental results. Thus $Si(OH)_4$ is most likely the volatile species present in the lean-burn furnace tests.

Figure 6.4 shows the HPBR results at standard conditions for both fuel-lean and fuel-rich mixtures as compared with those obtained in furnace tests. The HPBR rates are much higher, however the furnace tests were performed at a much lower pressure and velocities (1 atm, 4.4 cm/s for fuel-lean, 0.44 cm/s for fuel-rich) than the rig tests. Using the parametric scaling factors (Equations 6.4 and 6.5), both the fuel-lean and fuel-rich furnace results are scaled to the burner rig conditions (dashed lines). There is good agreement between the HPBR and scaled TGA data for the fuel-lean $Si(OH)_4$ model, but the fuel-rich SiO model does not produce such agreement between the two. This suggests that in the case of the HPBR, the fuel-lean $Si(OH)_4$ model is again supported, however under rich-burn conditions there

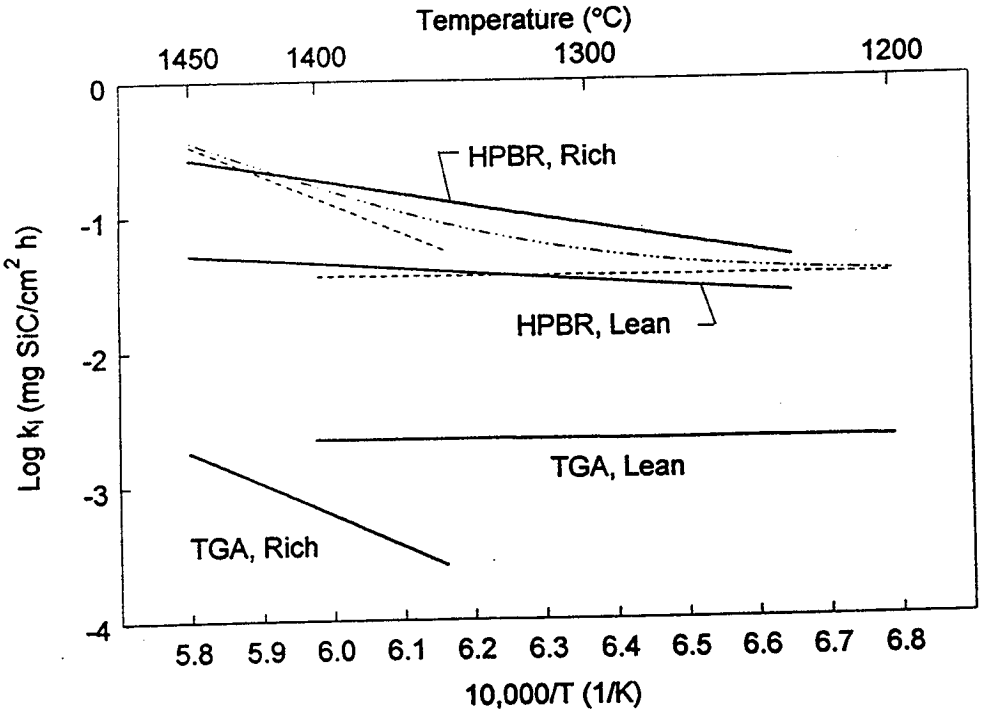

Figure 6.4 TGA recession rates as compared to HPBR results. In addition, TGA has been scaled to HPBR (dashed lines). Dotted-dashed line represents scaled TGA using a $SiO + Si(OH)_4$ model.

must be a species other than SiO operative. Figure 6.4 also shows a combined curve which represents the sum of the two TGA extrapolated lines, and the combined curve appears similar to the rich-burn curve obtained from the HPBR. Since the hydroxyl species can be formed in the rich regime, SiO_2 may volatilize in the HPBR as a combination of SiO + $Si(OH)_4$, or another unknown $SiO(OH)_x$ species. Recent unpublished work by Opila, shown in Figure 6.5, indicates that $Si(OH)_4$ should be formed at higher pressures and helps explain why SiO is was operative in the TGA.

Lastly, Figure 6.6 shows the boundary layer rates calculated for the $Si(OH)_4$ model under standard lean-burn conditions compared to HPBR results. Again, good agreement supports the presence of this species in the HPBR. Conversely, Figure 6.7 shows the similar theoretical predictions for SiO + $Si(OH)_4$ compared to rates obtained under fuel-rich HPBR conditions. Here, poor correlation reiterates that the exact volatile species under fuel-rich combustor conditions is unknown. Therefore, any theoretical predictions for potential engine conditions will not hold a high level of confidence.

6.3 Normalized Recession Rates

The boundary layer equation predicts that the HPBR Arrhenius curves for linear recession rates will scale with $(V_{g1}/V_{g2})^{1/2}$ and $(P_{t1}/P_{t2})^n$, where $n = 3/2$ for lean-burn and $n = -1/2$ for rich-burn, using the SiO and $Si(OH)_4$ models. These relationships are derived from Equations 6.4 and 6.5, by treating the partial pressures (P_{H2} and P_{H2O}) as a fractional amount of P_{Total}

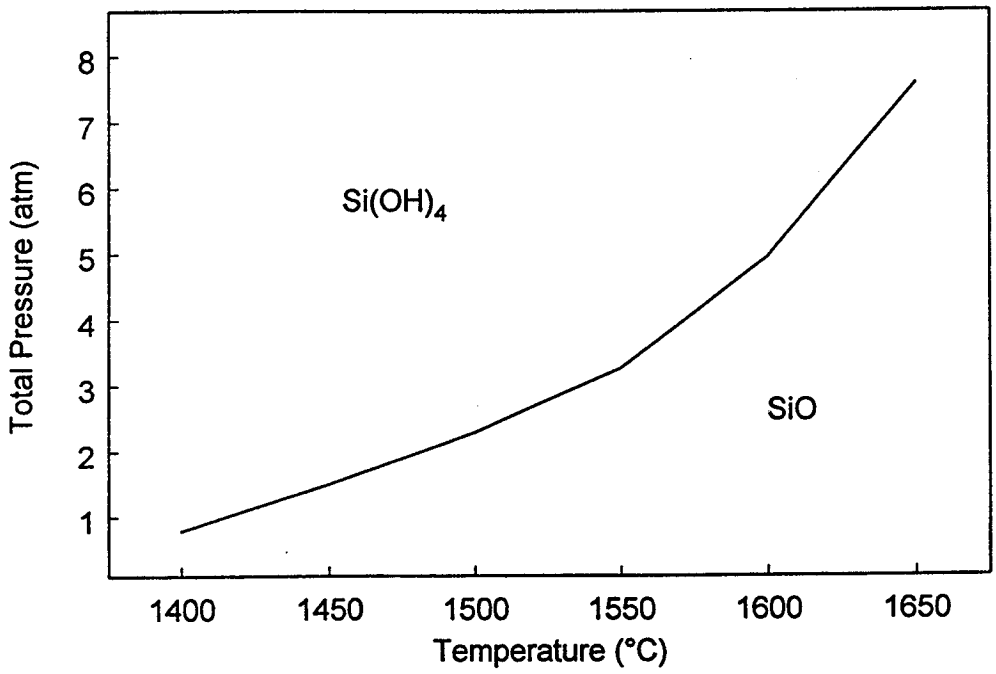

Figure 6.5 Predicted stability diagram of predominant volatile species over SiO_2 in a model fuel-rich gas mixture ($\phi = 1.4$) [Opila].

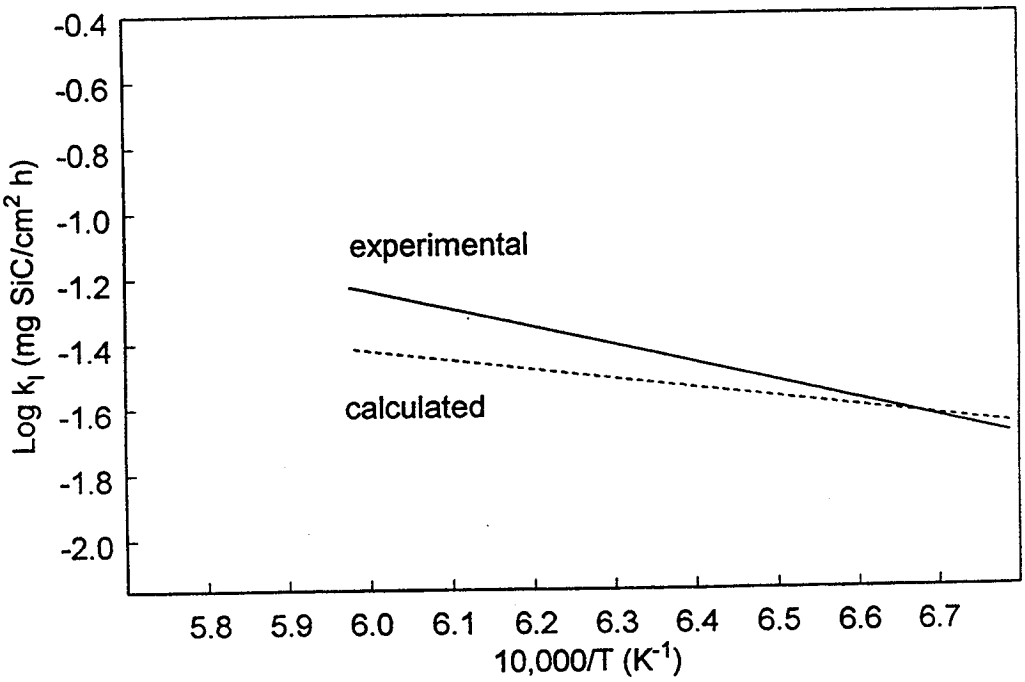

Figure 6.6 Lean-burn HPBR SiC recession rates compared to calculated boundary layer rates using the $Si(OH)_4$ chemical model [Opila].

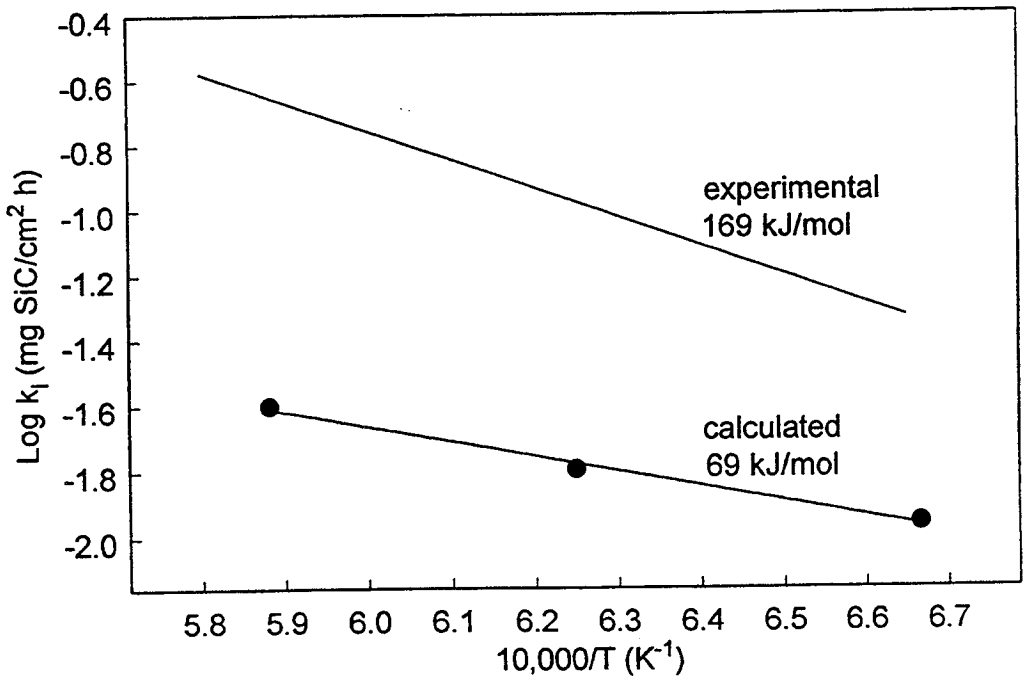

Figure 6.7 Rich-burn HPBR SiC recession rates compared to rates predicted using a $SiO + Si(OH)_4$ chemical model [Opila].

and dividing. Using this, the recession rates measured for HPBR standard conditions were compared to those under other HPBR pressures and velocities. As with TGA to HPBR comparisons, the same level of agreement with lean-burn conditions was not obtained for rich-burn conditions due to uncertainty in the exact chemical model. Therefore, additional analyses were performed to completely determine the pressure and velocity dependence of SiC recession for rich-burn, as well as lean-burn, conditions.

In the HPBR, the parameters T_s, P_t, and V_g cannot be adjusted as fully independent variables. Therefore, it is difficult to design an experiment to empirically define all the effects of temperature, pressure, and velocity. Given the uncertainty of the exact rich-burn chemical model and the limited experimental space of the HPBR, a precise parametric dependency is required to improve the accuracy of recession rate extrapolation to untested combustor conditions. All previous thermodynamic and boundary layer analyses suggest that the scale volatility of SiO_2 should vary with the operating temperature, pressure, and velocity according to an $\exp(\Delta E/RT)*P^xv^y$ dependence. It has also been shown that two different sets of ΔE, x, and y will be used to describe rich and lean combustor operation. Thus the concept of a normalized recession rate is explored.

As a result, all of the HPBR recession data was grouped into rich-burn and lean-burn data sets. Multiple linear regression was used to model the data in the form of the boundary layer equation dependencies. The resulting

dependencies are given as Equations 6.6 and 6.7 for rich and lean, respectively:

$$k_l(\text{rich}) = 82.5 \cdot [10^{-8324/T°C+273}] * P^{1.744} * v^{0.691} \quad \textbf{(6.6)}$$

$$k_l(\text{lean}) = 2.04 \cdot [10^{-5654/T°C+273}] * P^{1.504} * v^{0.497} \quad \textbf{(6.7)}$$

where k_l is mg/cm^2-hr, T is °C, P is atm, and v is m/s. As before, recession rates (μm/hr) can be obtained by multiplying the weight loss rates by 3.109.

For rich-burn, Equation 6.6 gives a $P^{1.74}v^{0.69}$ dependence, with an R^2 of 0.95 and activation energy of 159 kJ/mol. The slope of the rich-burn regression, -8324, has been left in the equation's exponential for clarity. A $P^{-0.5}v^{0.5}$ dependence was predicted for the volatile SiO species from the reaction between SiO_2 and H_2. Previous scaling of TGA results to HPBR conditions underestimated the rich-burn recession rates, especially at lower temperatures, because these dependencies and the activation energy are considerably different than the furnace (459 kJ/mol) and theoretical (520 kJ/mol) values. Again, the chemical effects simulated in the furnace tests were not reproduced in the HPBR, which further supports that additional or other species than SiO must be present.

For lean-burn, Equation 6.7 exhibits a $P^{1.50}v^{0.50}$ dependence, just as predicted for the volatile $Si(OH)_4$ species predicted for the reaction between SiO_2 and H_2O. Here, an R^2 of 0.98 and activation energy of 108 kJ/mol

were obtained. The activation energy is slightly higher than theoretical (57 kJ/mol) and furnace (3 kJ/mol) values, however the latter was subject to a large standard deviation. Given the P and v exponents generated by the multiple linear regression, confidence that the correct chemical model was chosen is extremely high, thus allowing confident extrapolations.

To show all the recession data as a function of T, P, and v on a single graph, the recession rates (k_l) are normalized by dividing by the appropriate P^xv^y factor. Figures 6.8 and 6.9 show normalized Arrhenius plots for rich and lean conditions, respectively. Operational pressures for each point are marked with the exception of standard (6-6.3 atm) conditions. As expected, linear regression gives results similar to Equations 6.6 and 6.7, with slight differences in pre-exponential, exponential exponent, and R^2 values. The data for the fuel-rich falls within $\pm 50\%$ of the regression value, and the fuel-lean within $\pm 25\%$. This indicates the scatter involved and provides a confidence level for projecting recession for other conditions. The equations for Figures 6.8 and 6.9 are for plotting purposes only, thus any prediction of SiC recession should be made using Equations 6.6 and 6.7.

In general, both rich and lean recession exhibit close to a $P^{1.5}v^{0.5}$ dependence which confirms that the hydroxyl $Si(OH)_4$ species, or some other $SiO(OH)_x$ species, most likely plays an important role in SiC recession for both fuel-rich and fuel-lean combustion. A comparison of rich-burn and lean-burn recession, normalized by this $P^{1/2}v^{1/2}$ factor in both cases, is

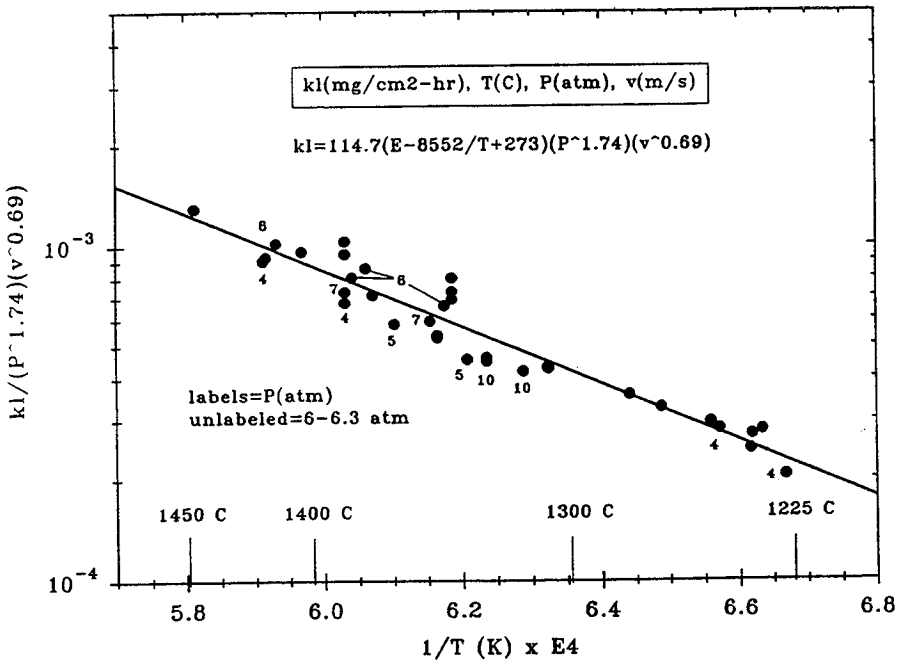

Figure 6.8 Normalized HPBR recession rates from multiple linear regression for rich-burn conditions (1225-1450°C, 4-10 atm, 15-27 m/s).

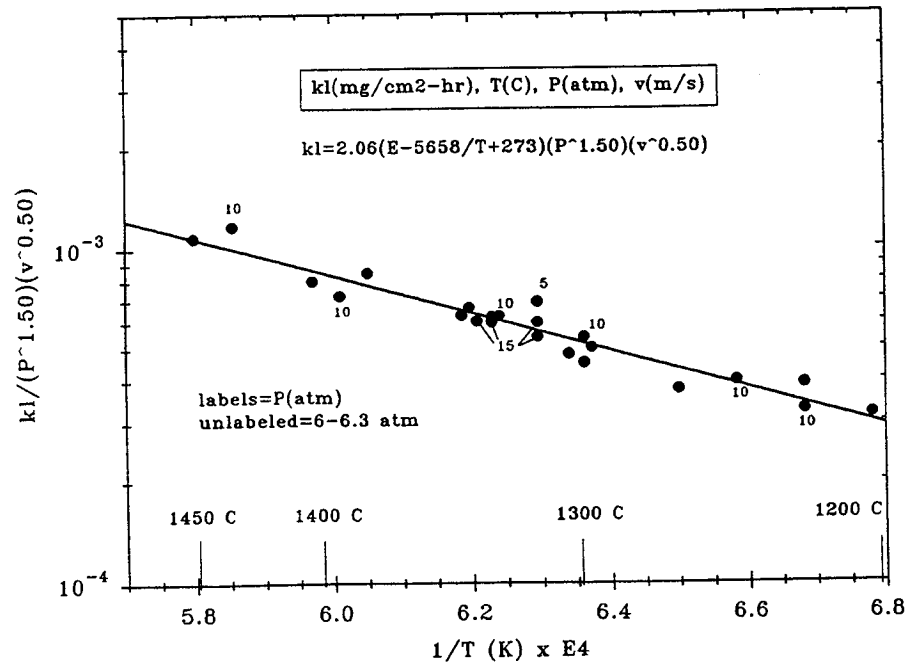

Figure 6.9 Normalized HPBR recession rates from multiple linear regression for lean-burn conditions (1200-1450°C, 5-15 atm, 10-23 m/s).

shown in Figure 6.10. Here, with both rich-burn and lean-burn data all on a single plot, the higher SiC recession rates and greater temperature dependence under fuel-rich conditions are clearly shown. Again, the equations generated by these multi-linear regressions correspond very well with previous regressions, suggesting very similar activation energies.

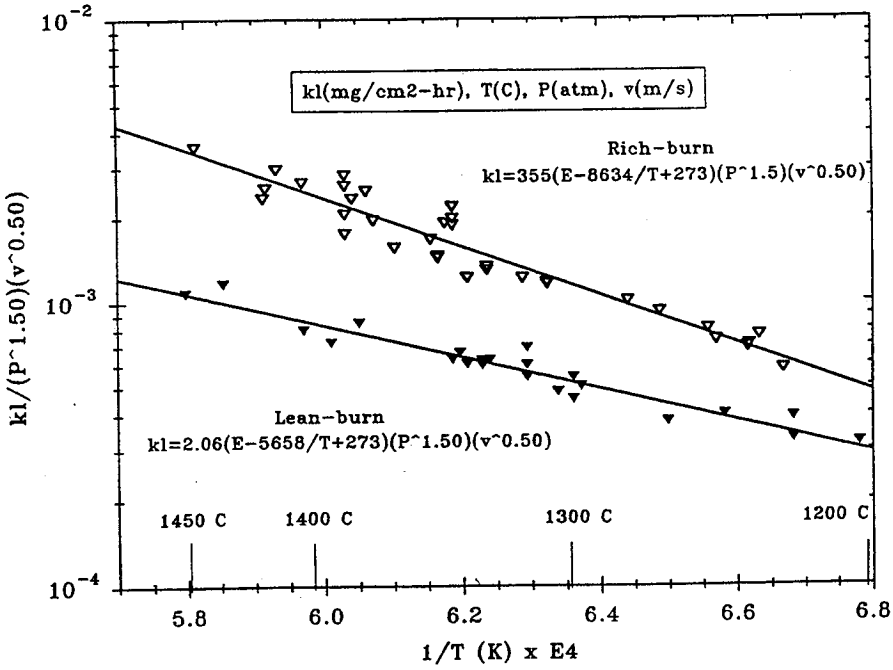

Figure 6.10 Normalized HPBR recession rates using $P^{1/2}v^{1/2}$ dependency.

6.4 Projected Recession under Gas Turbine Conditions

As stated, potential engine conditions (pressure and velocity) may be slightly different than HPBR experimental conditions. With the development of the multiple linear regression equations, SiC recession rates, which could not previously be predicted with a high degree of confidence, can now be predicted more accurately for untested conditions. For best accuracy, it is recommended that predictions be made for conditions within the HPBR experimental range.

To illustrate the significance of this recession, Table 6.1 gives the predicted SiC recession for 1000 hours as a function of temperature for two sets of generic engine conditions. Examples of both lean-burn (10 atm, 90 m/s) and rich-burn (10 atm, 30 m/s) engine conditions are given, and these engines are assumed to operate with equivalence ratios similar to those in the HPBR. Here, a 254 μm (10 mil) layer of a SiC combustor liner would be consumed in only 1000 hours of operation at 1200°C for both engines. This falls significantly short of a required 18,000 hour life combustor. Furthermore, a 0.3 cm (⅛ in.) combustor liner would be completely consumed in less than 12,000 hours of operation at 1200°C for either engine.

Table 6.1 - Projected SiC recession (μm/1000 hrs) under generic lean-burn and rich-burn engine conditions.

TEMP (C)	Lean-burn (10 atm, 90 m/s)	Rich-burn (10 atm, 30 m/s)
1000	69	43
1100	144	129
1200	275	333
1300	482	762
1400	791	1579
1500	1226	3012

7.0 CONCLUSIONS

SiC exhibits linear weight loss and surface recession as a function of time during exposure to both fuel-lean and fuel-rich combustion conditions. This is the first time this phenomenon has been documented in burner rig tests. The recession of SiC is a result of the SiO_2 oxide scale reacting with combustion products to form volatile gas species. This reduces the oxide scale according to paralinear kinetics, defined as simultaneous oxidation behavior and linear volatilization. Increased temperature accelerates the SiO_2 volatility, with the rates following an Arrhenius-type behavior. In addition to temperature, the volatility also increases with pressure and velocity.

The burner rig results agree well with TGA data for fuel-lean gas mixtures, but there are discrepancies with the fuel-rich correlation. This is supported by theoretical comparisons. As a result, there is high confidence in the $Si(OH)_4$ model being suggested for lean-burn conditions, where H_2O is the primary reactant. However, the exact chemical model is unknown for rich-burn conditions, but it is suspected to be some form of SiO and/or $Si(OH)_4$, in which H_2 may also be a reactant. Without the confidence for theoretical modeling, normalized HPBR data gives precise parametric dependencies that best predict SiC recession for untested combustor conditions. Severe SiC recession is predicted for potential conditions of future combustors. The use of SiC for these applications may still be feasible, however a environmentally protective coating may be required.

REFERENCES

1. J. Cramer, Supersonic Boom, Time, September 30, 1991, pp.48-49.

2. A. Kumar Naj, GE and Pratt Hope to Outdo the Concorde Jet, Wall Street Journal, October 10, 1990.

3. A.K. Gupta and D.G. Lilley, Combustion and Environmental Challenges for Gas Turbines in the 1990's, AIAA 91-1964, June 1991.

4. J. Ott, Researchers Seek Technology for Quiet Environmentally Safe SST, Av. Week Space Technol., vol. 132, no. 25, June 18, 1990, pp.94-95,98.

5. G.E. Allen, et al., Benefit of Advanced Materials in Future High Speed Civil Transport Propulsion Systems, NASA Contractor Report 185246, July 1990, pp.50-51.

6. N.S. Jacobson, High Temperature Durability Considerations for HSCT Combustor, NASA Tech. Paper 3162, January 1992.

7. A.H. Lefebvre, Pollution Control in Continuous Combustion Engines, School of Mech. Engr., Cranfield Instit. of Tech., England.

8. N.J. Shaw, et al., Materials for Engine Applications Above 3000°F-An Overview, NASA TM-100169, 1987.

9. N.S. Jacobson, J.L. Smialek, D.S. Fox, E.J. Opila, Durability of Silica-Protected Ceramics in Combustion Atmospheres, in High-Temperature Ceramic-Matrix Composites I, ed. by A.G Evans and R. Naslain, American Ceramic Society, Westerville, Ohio, 1995, pp.158-163.

10. Q.N. Nguyen, Carbon Dioxide Oxidation of Silicon Carbide, unpublished.

11. B.E. Deal and A.S. Grove, General Relationship for the Thermal Oxidation of Silicon, J. Appl. Phys., vol. 36, 1965, pp.3770-3778.

12. M.C. Cheng and I.B. Cutler, Vaporization of Silica in Steam Atmospheres, J. Am. Ceram. Soc., vol. 62, no. 11, 1979, pp. 593-596.

13. A. Hashimoto, The effect of H_2O gas on volatiles of planet-forming major elements: I. Experimental determination of the thermodynamic properties of Ca-, Al-, and Si-hydroxide gas molecules and its application to the solar nebula, Geochim. et Cosmochim. Acta, vol. 56, 1992. pp.511-532.

14. N.S. Jacobson, Oxidation and Corrosion of Silicon-based Ceramics-Challenges and Critical Issues, in preparation.

15. E.J. Opila, D.S. Fox, and N.S. Jacobson, Mass Spectrometric Observations of $Si(OH)_4(g)$, in preparation.

16. E.J. Opila and N.S. Jacobson, SiO(g) Formation from SiC in Mixed Oxidizing/Reducing Gases, in press Oxid. Met.

17. E.J. Opila and R.E. Hann, Paralinear Oxidation of CVD SiC in Water Vapor, submitted to J. Am. Ceram. Soc.

18. D.S. Fox, E.J. Opila, and R.E. Hann, Paralinear Oxidation of CVD SiC in a Simulated Rich-Burn Environment, in preparation for the J. Am. Ceram Soc.

19. C.A. Stearns and R.C. Robinson, NASA Lewis Research Center Lean-, Rich-Burn Materials Test Burner Rig, NASA Contractor Report 194437, February 1994.

20. R.A. Brady and G.S. Samuelsen, Visualization of Dome Region Mixing in a Quartz Combustor, ASME Paper 91-GT-360, 1991.

21. A.H. Lefebvre, Gas Turbine Combustion, Hemisphere Publishing, New York, 1983, p.66.

22. R. Browning, J.L. Smialek, and N.S. Jacobson, Multielement Mapping of α-SiC by Scanning Auger Microscopy, Adv. Ceram. Mat., vol. 2, no. 4, 1987.

23. C.R. Barrett, W.D. Nix, and A.S. Tetelman, The Principles of Engineering Materials, Prentice-Hall, Englewood Cliffs, NJ, 1973, p.148.

24. D.W. Richerson, Modern Ceramic Engineering, Dekker, New York, 1992, pp.19-23.

APPENDIX A

CARBON MONOXIDE FUME INCINERATOR

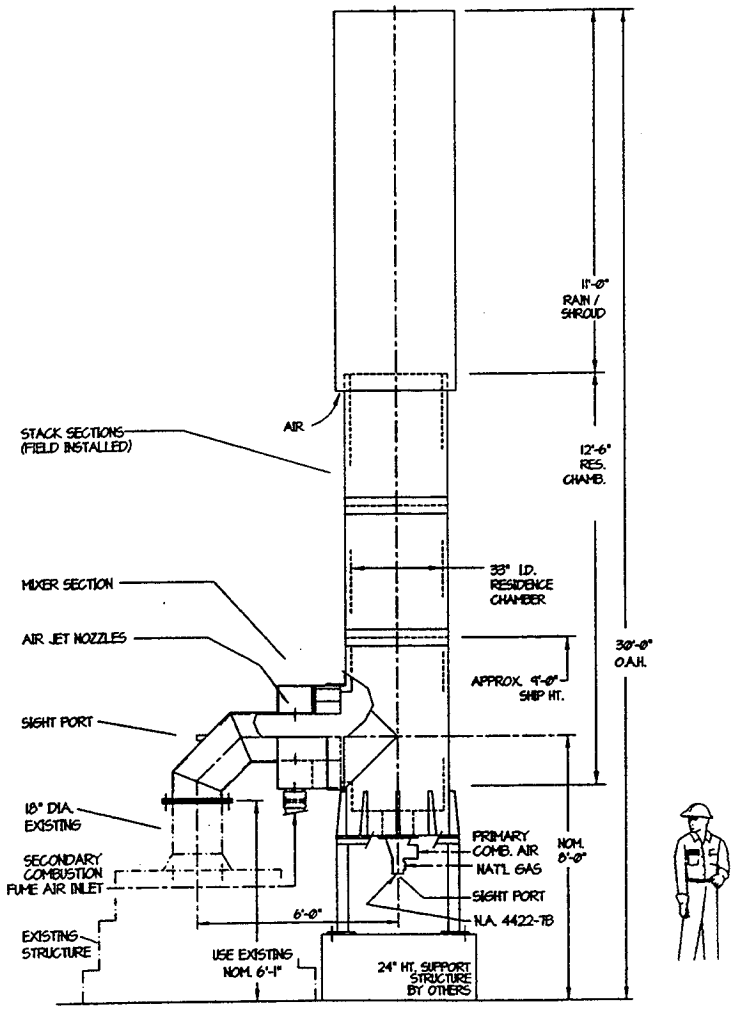

REPORT DOCUMENTATION PAGE

Form Approved
OMB No. 0704-0188

1. AGENCY USE ONLY (*Leave blank*)	2. REPORT DATE	3. REPORT TYPE AND DATES COVERED
	March 1997	Final Contractor Report

4. TITLE AND SUBTITLE

SiC Recession Due to SiO_2 Scale Volatility Under Combustor Conditions

5. FUNDING NUMBERS

WU–537–04–22
C–NAS3–27186

6. AUTHOR(S)

Raymond Craig Robinson

7. PERFORMING ORGANIZATION NAME(S) AND ADDRESS(ES)

NYMA, Inc.
2001 Aerospace Parkway
Brook Park, Ohio 44142

8. PERFORMING ORGANIZATION REPORT NUMBER

E–10685

9. SPONSORING/MONITORING AGENCY NAME(S) AND ADDRESS(ES)

National Aeronautics and Space Administration
Lewis Research Center
Cleveland, Ohio 44135–3191

10. SPONSORING/MONITORING AGENCY REPORT NUMBER

NASA CR–202331

11. SUPPLEMENTARY NOTES

This report was submitted as a thesis in partial fulfillment of the requirements for the degree Master of Science to the Case Western Reserve University, Cleveland, Ohio, May 1996. Project Manager, Leslie A. Greenbauer-Seng, Materials Division, NASA Lewis Research Center, organization code 5160, (216) 433–6781.

12a. DISTRIBUTION/AVAILABILITY STATEMENT

Unclassified - Unlimited
Subject Category 27

This publication is available from the NASA Center for AeroSpace Information, (301) 621–0390.

12b. DISTRIBUTION CODE

13. ABSTRACT (*Maximum 200 words*)

One of today's most important and challenging technological problems is the development of advanced materials and processes required to design and build a fleet of supersonic High Speed Civil Transport (HSCT) airliners, a follow-up to the Concorde SST. The innovative combustor designs required for HSCT engines will need high-temperature materials with long-term environmental stability. Higher combustor liner temperatures than today's engines and the need for lightweight materials will require the use of advanced ceramic-matrix composites (CMC's) in hot-section components. The HSCT is just one example being used to demonstrate the need for such materials. This thesis evaluates silicon carbide (SiC) as a potential base material for HSCT and other similar applications. Key issues are the enviromental durability for the materials of interest. One of the leading combustor design schemes leads to an environment which will contain both oxidizing and reducing gas mixtures. The concern is that these environments may affect the stability of the silica (SiO_2) scale on which SiC depends for environmental protection. A unique High Pressure Burner Rig (HPBR) was developed to simulate the combustor conditions of future gas turbine engines, and a series of tests were conducted on commercially available SiC material. These tests are intended as a feasibility study for the use of these materials in applications such as the HSCT. Linear weight loss and surface recession of the SiC is observed as a result of SiO_2 volatility for both fuel-lean and fuel-rich gas mixtures. These observations are compared and agree well with thermogravimetric analysis (TGA) experiments. A strong Arrhenius-type temperature dependence exists. In addition, the secondary dependencies of pressure and gas velocity are defined. As a result, a model is developed to enable extrapolation to points outside the experimental space of the burner rig, and in particular, to potential gas turbine engine conditions.

14. SUBJECT TERMS

SiC Oxidation; SiO_2 Volatiles

15. NUMBER OF PAGES

102

16. PRICE CODE

A06

17. SECURITY CLASSIFICATION OF REPORT	18. SECURITY CLASSIFICATION OF THIS PAGE	19. SECURITY CLASSIFICATION OF ABSTRACT	20. LIMITATION OF ABSTRACT
Unclassified	Unclassified	Unclassified	